Chemometrics and Intelligent Laboratory Systems 261 (2025) 105377

Contents lists available at ScienceDirect

Chemometrics and Intelligent Laboratory Systems

journal homepage: www.elsevier.com/locate/chemometrics

Optimizing adsorption efficiency: A novel application of SVM_Boosting_IGWO for methylene blue dye removal using low-cost fruit peels adsorbents

Nasma Bouchelkia [a,b,*], Hichem Tahraoui [c,d,e,j], Kheira Benazouz [b], Amal Mameri [b], Reguia Boudraa [f], Hamza Moussa [b], Nadia Hamri [b], Ryma Merdoud [b], Hayet Belkacemi [g], Abdelhalim Zoukel [i,h], Abdeltif Amrane [j], Mohammed Kebir [k], Lotfi Mouni [b]

[a] Centre de Recherche en Technologies Agro-Alimentaires, Route de Targa Ouzemmour, Campus Universitaire, Bejaia 06000, Algeria
[b] Laboratory of Management and Valorization of Natural Resources and Quality Assurance, SNVST Faculty, Akli Mohand Oulhadj University, Bouira, 10000, Algeria
[c] Reaction Engineering Laboratory, Faculty of echanical and Process Engineering, University of Science and Technology Houari Boumediene, BP32 El Alia, Bab Ezzouar, Algiers, 16111, Algeria
[d] Laboratory of Biomaterials and Transport Phenomena (LBMPT), University of MÉDÉA, Algeria
[e] Nouveau Pôle Urbain, Médéa University, 26000, Médéa, Algeria
[f] Laboratory of Materials and Durable Development (M2D), University Bouira, 1000, Bouira, Algeria
[g] Technology Laboratory of Materials and Process Engineering (LTMGP), University of Bejaia, 06000, Bejaia, Algeria
[h] Laboratory Physico-Chemistry of Materials, Laghouat University, 03000, Laghouat, Algeria
[i] Center for Scientific and Technical Research in Physicochemical Analysis (PTAPC, Laghouat-CRAPC), 03000, Laghouat, Algeria
[j] Univ Rennes, Ecole Nationale Supérieure de Chimie de Rennes, CNRS, ISCR – UMR6226, F-35000, Rennes, France
[k] Research Unit on Analysis and Technological Development in Environment (URADTE-CRAPC), BP 384, Bou-Ismail, Tipaza, 42004, Algeria

ARTICLE INFO

Keywords:
Biosorption
Improved grey wolf optimizer
Methylene blue
Orange peel
Potato peel
Support vector machine

ABSTRACT

In this work, the potential for employing orange peels (OP) and potato peels (PP) as biosorbents to remove the methylene blue dye (MB) from aqueous solutions is studied. Several physicochemical methods, such as FTIR, SEM-EDX, X-ray diffraction, and pH point of zero charge measurement, were used to analyze the adsorbents. FTIR analysis revealed changes in peak intensities after dye adsorption. SEM analysis confirmed the presence of starch in the PP adsorbent, while no apparent pore structure was observed in the OP adsorbent. EDX analysis showed that carbon and oxygen were the main components on the surfaces of OP and PP. X-ray diffraction patterns indicated that both adsorbents were amorphous materials. The impact of different factors, including adsorbent dosage, contact time, temperature, initial dye concentration, pH and particle size, on the biosorption process was studied. Kinetic studies revealed that equilibrium was reached within a few minutes of contact, and the MB removal followed the pseudo-second-order model.Furthermore, a novel predictive model combining Support Vector Machine (SVM) with Boosting and the Improved Grey Wolf Optimizer (IGWO) algorithm was developed. The SVM-IGWO-Boosting model exhibited excellent performance in predicting methylene blue adsorption, demonstrating perfect correlation and low prediction error. The IGWO optimization approach effectively optimized the input parameters for the adsorbents, resulting in excellent agreement between experimental and predicted values. Moreover, OP showed higher efficiency in removing methylene blue compared to PP, with a maximum capacity of 111.75 mg/g for OP and 96.67 mg/g for PP using IGWO. The use of orange peels and potato peels as agricultural waste for methylene blue removal offers an efficient and sustainable solution. The SVM-IGWO-Boosting predictive model, in conjunction with the IGWO optimization approach, provides a promising tool for predicting and optimizing the adsorption efficiency of MB adsorbents. These findings present valuable prospects for real-world applications requiring accurate and reliable predictions.

* Corresponding author. Centre de Recherche en Technologies Agro-Alimentaires, Route de Targa Ouzemmour, Campus Universitaire, Bejaia, 06000, Algeria.
E-mail addresses: nasma.bouchelkia@crtaa.dz, nasma.bouchelkia@univ-bejaia.dz (N. Bouchelkia), hichemm.tahraouii@gmail.com (H. Tahraoui), kheira.benazouz@univ-bejaia.dz (K. Benazouz), a.mameri@univ-bouira.dz (A. Mameri), r.boudraa@univ-bouira.dz (R. Boudraa), h.moussa@univ-bouira.dz (H. Moussa), n.hamri@univ-bouira.dz (N. Hamri), r.merdoud@univ-bouira.dz (R. Merdoud), hayet.belkacemi@univ-bejaia.dz (H. Belkacemi), ab.zoukel@lagh-univ.dz (A. Zoukel), abdeltif.amrane@univ-rennes1.fr (A. Amrane), medkebir@yahoo.fr (M. Kebir), l.mouni@univ-bouira.dz (L. Mouni).

https://doi.org/10.1016/j.chemolab.2025.105377
Received 17 July 2024; Received in revised form 9 March 2025; Accepted 10 March 2025
Available online 10 March 2025
0169-7439/© 2025 Elsevier B.V. All rights are reserved, including those for text and data mining, AI training, and similar technologies.

1. Introduction

Synthetic dyes are widely used in process industries such as textiles, leather, cosmetics, food processing, pharmaceuticals, and paints, and about 10–15 % of the 0.8 million tonnes produced annually are released into the environment [1,2]. The dye industry is expected to develop by roughly 2–3 % every year owing to rising worldwide dye production and consumption [3]. The growing dye production results in toxic and carcinogenic byproducts, posing a serious threat to the ecosystem, aquatic life, and human health. [4–6]. Among these dyes, methylene blue is widely used for coloring materials, such us paper, wigs, and fabrics, as well as for biological staining. It also treats UTIs and methemoglobinemia. However, its accumulation in wastewater can be harmful human health, causing nausea, vomiting, diarrhea, and eye burns [7,8].

The treatment of dye effluents has been effectively achieved through various methods such as photocatalytic degradation, membrane filtration, irradiation, and conventional adsorption [3,9,10], biological treatment, ultrasonic-assisted adsorption, and coagulation and flocculation, photo Fenton degradation [11–15]. Among these methods, adsorption is widely used due to its simplicity, availability of adsorbents, selectivity, and scalability. The most popular adsorbent is activated carbon because of its effectiveness and large surface area. Many researchers have looked into biosorption as a low-cost, secure, and potentially effective alternative to conventional adsorbents [16]. Dyes removal using untreated biosorbents, biosorbents thermally processed, and/or sorbents activated using some chemical products [17,18] has been established in several studies. Agricultural waste products have the potential to be easily accessible, cost-effective, and effective adsorbents [19]. They also have a variety of other advantages that make them valuable tools for environmental conservation, including a good selectivity for a range of concentrations, a substantial adsorption capacity, abundance, renewability and rapid kinetics. Agricultural wastes perform better than other adsorbents as they are frequently used with little to no preparation and generally do not require heat treatment, lowering then the manufacturing costs and saving energy [20–22].

Recent studies have investigated the use of fruit peels such as mango peels [23], pomelo peels, banana peels and mangosteen peels [24], Prunus spinosa L. fruit pulp [25], pomegranate (Punicagranatum) peels [26], grapefruit peels [27], lemon peels [28], jackfruit peels [29], durian peels [30], and dragon fruit foliage [31] for the adsorption-based removal of MB pollutant from aqueous solutions.

The potential of using orange and potato peels as adsorbents for dye removal has been widely explored [32–35]. Due to their high global consumption, these fruits generate large amounts of unutilized and unprocessed peels, leading to significant waste. According to the FAO report [36], potato production reached 383 million tonnes in 2023, an increase of 17 % since 2010, while orange production was estimated at 70 million tonnes. This growth is particularly evident in developing regions, such as Africa, where potato production has reached 26 million metric tons [37]. To address the issue of agricultural waste, researchers have investigated various methods of reusing these by-products. In addition to their application as adsorbents, orange and potato peels have been studied for their potential in sustainable processes. Açıkalın [38] investigated their use as raw materials in the pyrolysis process, to produce sustainable fuels and chemicals. Kamboj and Ms [39] examined the production of biobutanol from potato peel waste using Clostridium acetobutylicum in a diluted orange peel extract. Hanafi et al. [40] investigated the adsorption of methylene blue using activated carbon derived from a mixture of orange peel and watermelon rind, activated with $ZnCl_2$ under microwave treatment.

The objective of this work is to establish a low-cost biosorption method that can effectively and sustainably remove MB dye from aqueous solution applying potato and orange peels as adsorbents. In order to accomplish this, many of adsorption-related factors, such as pH, particle size, temperature, adsorbent dosages, MB initial concentration, and contact time have been investigated. Additionally, to evaluate the functional groups involved in MB uptake by OP and PP, Fourier-transform infrared spectroscopy analyses was also carried out. For a complete understanding of the adsorption behavior, the modeling of kinetics, adsorption isotherms, thermodynamic parameters, and reaction mechanisms has been thoroughly detailed.

To predict the adsorption behavior of MB on orange and potato peels, a modeling approach based on Support Vector Machine (SVM), Boosting, and Improved Grey Wolf Optimization (IGWO) was developed. This approach accounts for complex nonlinear relationships between input variables and adsorption performance, allowing the identification of optimal conditions to maximize biosorption efficiency. The SVM model is a supervised learning algorithm used for classification and regression, capable of handling complex datasets and discovering nonlinear relationships between input and output variables. Boosting is a machine learning technique that combines multiple weak models to form a strong model, enhancing prediction accuracy and stability. IGWO optimization is a grey wolf social behavior-inspired optimization method that models the hunting mechanism of grey wolves to find the best model parameters. This approach efficiently explores the parameter space and identifies optimal conditions to maximize adsorption performance. By comparing the performance of orange and potato peels in terms of MB dye removal rate, their effectiveness as adsorbents was evaluated.

The work presented in this study brings several innovations and significant advancements in the field of water pollution remediation. Firstly, an innovative approach was adopted to remove MB dye by using potato and orange peels as affordable adsorbents. These materials were chosen due to their easy availability, low cost, and agricultural waste status, making them an economically viable and environmentally friendly solution. Additionally, this study introduces significant innovations in the modeling and optimization of adsorption processes for water pollution remediation. A novel hybrid approach combining SVM, Boosting, and IGWO was developed to analyze experimental adsorption data. This advanced modeling framework effectively captures complex nonlinear relationships between input variables and adsorption performance, offering superior predictive accuracy compared to conventional methods. The integration of SVM, Boosting, and IGWO represents a pioneering effort, making this study the first to apply such a combination for the biosorption of MB dye using orange and potato peels as adsorbents. This innovative technique not only enhances the reliability of adsorption isotherm predictions but also provides a robust tool for optimizing operational parameters. The methodological advancements presented here pave the way for broader applications in adsorption systems, contributing to the development of more efficient and data-driven solutions for water pollution remediation.

2. Materials and methods

All chemicals used in this study were laboratory grade. The methylene blue used in this work ($C_{16}H_{18}N_3SCl$, Mw = 319.85 g mol^{-1}) is a basic (cationic), aromatic, heterocyclic synthetic dye belonging to the thiazine dye family [41–44]. It was purchased from Biochem Chemopharma (Cosne-Cours-sur-Loire, France). A stock solution of 1000 mg/L MB was prepared using deionised water. Working solutions were obtained by dilution to the desired concentrations.

2.1. Preparation and characterization of PP and OP adsorbents

In this study, OP and PP were sourced from a grocery vegetable market in Bouira, Algeria. The samples were repeatedly cleaned with tap water, rinsed with distilled water, dried in a hot air oven at 40 °C for 48 h, then crushed and sieved to a particle size of <100 μm. The OP and PP samples were finally stored in airtight containers for later use, without undergoing any further chemical or physical treatment prior to the sorption experiments. The humidity rate, the ash content, the iodine index, pH point zero charge (pHpzc), the chemical groups (Boehm

titration), and the apparent density were determined (see supplementary material).

The determination of the methylene blue index and the surface area available to methylene blue was carried out using the method outlined in our previous study [45].

2.2. FTIR analysis

OP and PP adsorbent surfaces were examined using an FTIR spectrometer with a PerkinElmer FTIR 1000 spectrometer (Version 10.4.1) at room temperature, to identify the functional groups. It was not necessary to pre-treat the adsorbent powders before performing the analysis. The spectra were captured between 4000 cm^{-1} and 400 cm^{-1}, with a resolution of 1 cm^{-1}.

2.3. Scanning electron microscopy (SEM) and EDX analysis

SEM is a powerful analytical tool for observing microscopic and nanoscopic structures that are invisible to the naked eye or optical microscopy. It uses electrons to examine samples, and generates images by collecting different signals generated by the interaction of electrons with the sample, offering a detailed view of the topography, morphology, composition and crystallographic information [46].

To analyze the morphology of the OP and PP adsorbents, a Thermoscientific Quattro S scanning electron microscope (ThermoFisher Scientific, USA) was employed. The main elements present on the surfaces of the adsorbents were detected using energy-dispersive X-ray spectroscopy (EDX). The analysis was performed with an EDAX Octane Elect detector. The quantification of data was performed using Genesis™ software, with an acquisition time of approximately 2 min per spectrum.

2.4. X-ray diffraction (XRD) analysis

X-ray diffraction (XRD) characterizes crystalline materials, revealing their structure, phases and atomic arrangement. Diffraction peaks are the result of the constructive interference of X-rays reflected at specific angles from the crystal lattice planes of the sample [47,48]. The structural features of the materials were examined using XRD analysis, with a Malvern Panalytical X'pert Pro analyzer (Almelo, Netherlands) operating at room temperature, the XRD patterns were captured, and a 0.02 step was used to explore the structure analysis of OP and PP between 2θ angles of 10–80°.

2.5. Batch equilibrium and kinetic studies

All adsorption experiments performed in this work were carried out in a closed stirred reactor. The experimental setup consisted of an Erlenmeyer flask placed on a multi-position magnetic stirrer (2 Ma g Magnetic Motion and Selecta Multimatic-5N). Stirring was achieved using a magnetic bar to ensure good contact between the adsorbent and adsorbate. A series of adsorption studies were conducted, using various amounts of orange and potato peel (ranging from 0.2 to 5 g) and various concentrations of MB solutions (20, 50, 100, and 150 mg/L). The agitation speed was fixed to 200 rpm.

In order to study the effect of the parameters, the experiments were carried out by mixing 0.02 g of each adsorbent with 20 ml of MB solution and stirred for 180 min at a temperature of 25 ± 5 °C. The temperature verification was performed using an Isolab glass thermometer. Once the adsorption period was complete, the solution was centrifuged at 3000 rpm for 15 min using an LW Scientific EZ Swing centrifuge. The final concentration of the residual dye was determined at the maximum MB wavelength (668 nm), using an Optizen spectrophotometer (3220 UV, Mecasys, Korea). The pH was adjusted using 0.1 M HCl and NaOH solutions, with a Mettler Toledo FiveEasy F20 pH meter. At each initial concentration, the amount of dye adsorbed at any time (qt) and at equilibrium (qe) was determined using the following equations, respectively.

$$q_t = \frac{(C_0 - C_t)}{m} \times V \quad (1)$$

$$q_e = \frac{(C_0 - C_e)}{m} \times V \quad (2)$$

The removal efficiency (R%) of methylene blue was determined using equation (3)

$$R\ (\%) = \frac{(C_0 - C_t)}{C_0} \times 100 \quad (3)$$

Where C_0 and Ce (mg/L) are the concentrations of dye in liquid phase at initial time and at equilibrium, respectively. Ct (mg/L) are the concentrations of dye liquid phase at any time t, V (L) is the volume of the solution and m (g) is the used adsorbent mass [49,50].

2.6. Coupling Support Vector Machine with coupled with Boosting and Improved Grey Wolf Optimizer algorithm

The Support Vector Machine (SVM) is a powerful and widely used prediction algorithm [12]. It seeks to find an optimal hyperplane that separates data in a high-dimensional space [51]. The goal of SVM is to maximize the margin between samples of different classes while minimizing classification error [52]. This method relies on the use of support vectors, which are data points closest to the decision boundary [12]. However, Boosting is a machine learning technique that combines multiple weak learning models to form a stronger model [53]. They use an iterative approach to adjust successive models by focusing on samples that were poorly predicted by the previous models. This focus on errors can help reduce overfitting by paying more attention to challenging regions of the data space [52]. By combining SVM and Boosting, we can leverage the strengths of both approaches (SVM_Boosting). SVM can be used as a weak model in the Boosting process. At each iteration of Boosting, an SVM is trained on a subset of the data, focusing on difficult-to-classify samples. This combination enhances the capabilities of SVM by putting more emphasis on complex decision regions. Coupling SVM with Boosting offers several advantages. Firstly, it can tackle more complex classification problems by leveraging the separation capabilities of SVM and progressively improving results through Boosting. Additionally, this approach can help prevent overfitting by focusing on difficult samples rather than all samples.

In this study, an enhanced model using an SVM-Boosting model was developed to surpass conventional methods for forecasting the amount of MB adsorbed on OP and PP adsorbents.

Each adsorption time instant's findings for the adsorbed amount of MB were compiled into a database with the dimensions [236:7], which contained six input parameters and one output parameter. Contact time, adsorbent mass, MB concentration, pH, temperature, and adsorbent type were the independent parameters; they were denoted by values "1″ and "2″ for OP and PP, respectively. The output variable was the flow rate, representing the amount of MB adsorbed for each instant on the two adsorbents.

The SVM-Boosting model was designed and optimized to produce the best possible results. Using MATLAB's "mapminmax" function, the database was first normalized within the range [−1, +1]. Then, a training set (containing 70 % of the data) and a validation set (containing 30 % of the samples) were created from the database. The Gaussian kernel function was chosen for the SVM model due to several advantages. Firstly, it is capable of solving non-linear problems by transforming the input space into a higher-dimensional space, allowing the SVM model to be more flexible and capture complex relationships between variables. Moreover, the Gaussian kernel function is considered universal, meaning it can approximate any decision function with sufficient training data. It is also robust to outliers, reducing their impact on

the decision function. The sigma parameter of the kernel function can be adjusted to find a good compromise between model flexibility and the risk of overfitting. By combining these features, the Gaussian kernel function is widely used for modeling complex relationships, solving non-linear problems, and effectively handling outliers in SVM models.

The specific parameters of the Gaussian kernel function, such as Box-Constraint and sigma, were optimized using the Improved Grey Wolf Optimizer (IGWO) algorithm coupled with SVM (SVM-IGWO). The IGWO algorithm is an optimization method inspired by grey wolves social interaction and improves upon the Grey Wolf Optimizer (GWO) algorithm in terms of efficiency and convergence [54]. It utilizes a population of grey wolves in the search space and updates their positions based on formulas inspired by their social behavior [54]. The best wolves are also updated separately. The IGWO algorithm employs termination criteria to determine the end of optimization and has demonstrated its effectiveness in various domains, including engineering and machine learning. Then, the Boosting process was performed 30 times to train an initial weak model, giving more weight to misclassified samples to focus on errors. Then, another weak model was trained focusing on previous errors. This procedure was repeated multiple times to obtain a strong model.

Finally, a number of statistical metrics including the correlation coefficient (R), coefficient of determination (R^2), and root mean square error (RMSE) were used to assess the performance of the model and choose the best one [55–62]. Specific equations are used to compute these requirements.

$$R = \frac{\sum_{i=1}^{N}\left(y_{\exp}-\bar{y}_{\exp}\right)\left(y_{pred}-\bar{y}_{pred}\right)}{\sqrt{\sum_{i=1}^{N}\left(y_{\exp}-\bar{y}_{\exp}\right)^2\sum_{i=1}^{N}\left(y_{pred}-\bar{y}_{pred}\right)^2}} \tag{4}$$

$$R^2_{adj} = 1-\frac{(1-R^2)(N-1)}{N-K-1} \tag{5}$$

$$RMSE = \sqrt{\left(\frac{1}{N}\right)\left(\sum_{i=1}^{N}\left[\left(y_{\exp}-y_{pred}\right)\right]^2\right)} \tag{6}$$

Where N is the number of data samples; K is the number of variables (inputs); $\bar{y}_{\exp}$ and y_{pred} are the obtained experimental values and the predicted ones respectively; $\bar{y}_{\exp}$ and $\bar{y}_{pred}$ are respectively the average values of the experimental and the predicted values [63].

3. Results and discussion

3.1. Adsorbents characterization

The porosity development and the morphology of the OP and PP adsorbents were investigated by the SEM analysis. The obtained images are shown in Fig. 1.

The SEM image of the OP adsorbent (Fig. 1, A1) shows that there is no evidence of pore structure on the adsorbent surface, which displays a compact, smooth, irregular appearance with asymmetrically distributed granular particles [64]. The SEM image of PP ((Fig. 1, B1) showed the presence of spherical particles of different sizes uniformly distributed. A similar pattern was described by Hadadi et al. [35] confirming the presence of starch in the PP adsorbent. Based on the EDX analysis (Fig. 1, A2 and B2), C and O comprise the bulk of the OP and PP surfaces.

It was evident from the XRD analysis (Fig. 2) that both patterns showed no well-defined peaks, indicating the absence of a discrete mineral phase. The two peaks observed near 2θ = 17° and 22° are attributed to the distinctive crystal structures of starch and cellulose, respectively [65]. The broad peaks at 2θ around 15.77°, 19.51°, 21.29° and 24.50° reveal the amorphous nature of orange peel (OP) [66]. Consequently, the OP and PP are totally amorphous, as one would expect for organic materials.

Fig. 3 depicts the spectra from the analysis of the OP and PP functional groups before and after MB adsorption.

As evidenced by the infrared spectra (Fig. 3), the surfaces of the OP and the PP adsorbents contain a variety of functional groups, indicating their complex structure. The peaks at around 3400-3440 cm^{-1} correspond to O–H stretching vibration of hydroxyl groups. The peaks at 2929 cm^{-1} corresponds to the stretched vibration of a methyl group (-CH) of alkane chain [65]. The peaks at 1640 cm^{-1} for PP and 1629 cm^{-1} for OP are assigned to stretching vibrations of C═O bonds of carboxyl groups [45]. Phenolic O–H bending is represented by the band at roughly 1382 cm^{-1} [67]. C–O bonds of phenols, esters, ethers, and alcohols were appeared at around 1030 cm^{-1} for both adsorbents [68] and at 1159 cm^{-1} for the PP. The PP showed also peaks between 500 and

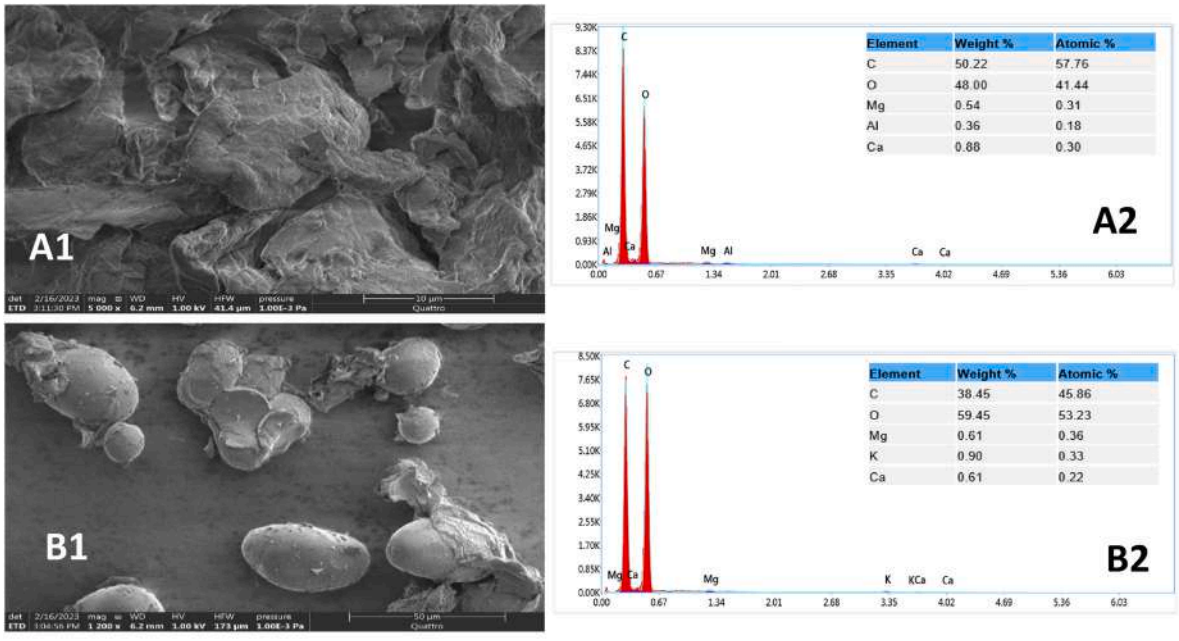

Fig. 1. SEM micrographs and EDX analysis of samples OP (A1, A2) and PP (B1, B2).

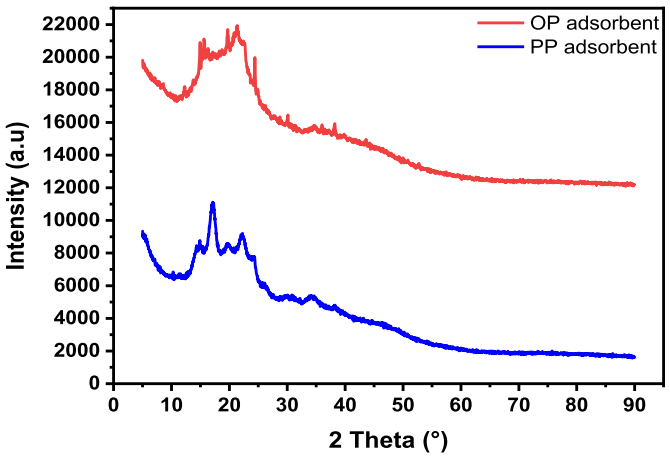

Fig. 2. X-ray diffraction graphs of the OP and PP adsorbents.

850 cm^{-1} related to the C–H bending [69]. The obtained results are in agreement with the findings of the EDX analysis which showed that the surface is predominantly composed of oxygen and carbon.

After MB adsorption, the position of some peaks was shifted to new position; the peaks at 2929 cm^{-1} were shifted to 2922 cm^{-1} for both adsorbents, and the band at 1159 cm^{-1} has shifted to 1165 cm^{-1} for the PP. the spectra show also that some bands' intensities were changed; the intensities of peaks at 3400-3440 cm^{-1}, 1640, 1629 and 1382 cm^{-1} has decreased. As a result, it can be concluded that the respective functional groups were responsible for the adsorption of MB dyes on both adsorbents. Same conclusion has been reported by Jawad et al., [70].

Table 1 shows some characteristics of OP and PP adsorbents.

According to Bouchelkia et al. [45], the amount of non-volatile and non-combustible components in a material is measured by its ash content. Ash content is low in effective adsorbents [71,72]. The least amount of ash was observed in OP (2.70 %).

The methylene blue index refers to the amount of methylene blue, in milligrams, adsorbed per gram of carbon [73]. It is a crucial parameter in characterizing an adsorbent's effectiveness. It also estimates the potential of OP and PP for the adsorption of large molecules such as MB. As can be observed in Table 2, the OP is characterized by higher MB index compared to PP, and therefore the highest specific MB surface area.

The iodine value quantifies the iodine uptake capacity of 1 g of adsorbent under specific conditions. A high iodine value demonstrates the effectiveness of the used adsorbent in removing small-size contaminants (microporous), and confirms its reliability in this regard [74]. The

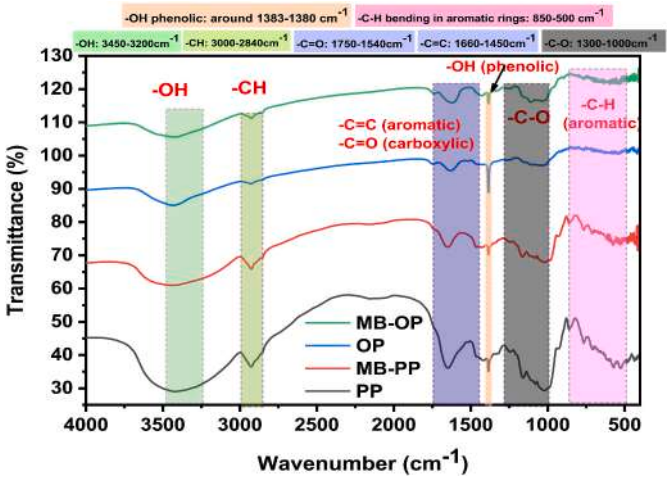

Fig. 3. FTIR spectrogram of samples of the OP and PP adsorbents.

Table 1
Characteristics of OP and PP.

Biomass	Orange peel (OP)	Potato peel (PP)
Humidity (%)	10.80	9.58
Ash content (%)	2.70	4.70
Apparent density (%)	0.76	0.62
MB index (mg/g)	111.05	71.66
specific surface (m^2/g)	271.85	175.42
iodine index (mg/g)	190.35	285.52

obtained value of iodine number for OP (190.35 mg/g) was lower than that for PP (285.52 mg/g). This suggests a higher abundance of microporous sites in PP compared to OP which may be more mesoporous due to the greater MB adsorption [75].

The pHpzc equates to the pH point at which the adsorbent surface has no net charge [76]. The curves permitting to determine the value of the pHpzc are depicted in Fig. 4.

A curve was drawn to reflect the equation $pH_{final} = f(pH_{initial})$. The pHpzc is equal to the solution pH for which the graph crosses the first bisector.

The $pH_f = f(pH_i)$ curve crosses the bisector at pH = 3.38 for OP and pH = 6.27 for PP. According to these values, the adsorbent surface is negatively charged at pH levels above (3.38 and 6.27) and positively charged at levels below (3.38 and 6.27) for OP and PP, respectively. As the pH increases above pHpzc, the negative ion density on the surface of OP and PP increases, allowing then the adsorption of MB cations by the electrostatic attraction phenomenon [77].

Boehm titration method is based on the idea that different base strengths can neutralize various acidities of oxygen groups on carbon surfaces [49]. Table 2 summarizes the total acidic and basic groups of both OP and PP. As can be observed from the results, the contents of acidic functions are much higher than those of basic functions in both materials. It has been demonstrated that the availability of more acidic sites, associated with a higher presence of oxygen groups, enhances the adsorption of cationic dyes [78]. This finding aligns with the MB index results, which indicate favorable MB adsorption due to the abundance of acidic functional groups.

3.2. *Effect of contact time and the initial adsorbate concentration*

The efficiency of the adsorption phenomenon is controlled by the contact time, which also serves to estimate the time needed to reach equilibrium. The effect of contact time on MB dye adsorption was evaluated using OP and PP adsorbents over varying durations (5–330 min) with an adsorbent dose of 1 g/L, and a temperature of (25 ± 0.5) °C, adjusted to the optimal pH of 7 ± 0.5. The curves corresponding to the adsorption kinetics of the two materials are represented in the following Figures.

The plotted curves show the evolution of the amount of dye adsorbed by potato and orange peels as a function of time, at different concentrations (20, 50, 80, 100, 150 mg/L). Both Figures show that the adsorption kinetics is fast during the initial few minutes of the adsorbent/adsorbate contact, which can be attributed to the accessibility of the adsorption sites [79]. Due to the repulsive interactions between the MB molecules adsorbed on the surface of the two adsorbents and the solution phase, the remaining unoccupied surface sites become more difficult to fill [3]. A plateau was eventually noticed, which matched the equilibrium between the two phases (solid and liquid) [80].

Table 2
BOEHM titration of OP and PP.

	Carboxylic -COOH	Lactonic -COO-	Phenolic OH	Total basicity	Total acidity
OP	0,63	0,65	0,63	0,86	1,91
PP	0,59	0,63	0,56	1,62	1,78

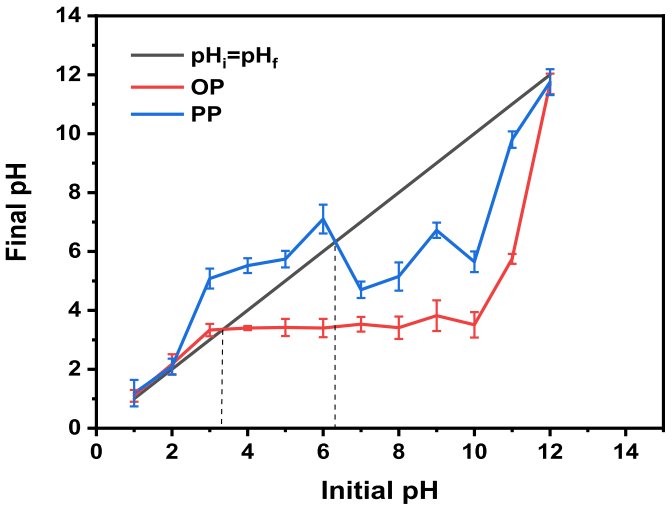

Fig. 4. PHpzc of orange peels (OP) and potato peels (PP). (For interpretation of the references to color in this figure legend, the reader is referred to the Web version of this article.)

Additionally, it is clear from the results that MB adheres to orange peels more quickly than to potato peels. This may be due to the higher surface area of OP (271.85 m^2/g) compared to PP (175.42 m^2/g), providing more available sites for MB adsorption.

The initial dye concentration was examined by varying the MB concentration from 20 to 150 mg/L. Figs. 5 and 6 show that increasing the MB initial concentration leads to the enhancement of the adsorbed quantity. The amount of MB adsorbed on OP and PP increased proportionally with the initial dye concentration. This can be explained by an increase in the gradient of solute concentration between the adsorbent surface and the solution [81]. This suggests that adsorption capacity is significantly influenced by the MB initial concentration.

3.3. Effect of adsorbent mass

Adsorption capacity is strongly affected by the amount of sorbent available in the liquid phase. The MB removal was evaluated in an adsorbent dosage range of 0.1–6 g/L.

The efficiency of MB removal as a function of adsorbent dosage is shown in Fig. 6. The quantity of adsorbed MB increases with the adsorbent dosage. For a dosage of 0.1 g/L of material, the removal efficiency reached 38.88 % for the OP and 22.99 % for the PP. The increase in adsorbent dosage enhances the MB removal rate by providing more active sites [82]. 1.5g of OP was enough to reach a maximum elimination of MB. In contrast, 3g of PP was required. Above these dosages, the adsorption rate remained nearly constant.

3.4. Effect of initial pH

Since adsorption is based on the driving force between the adsorbate and the adsorbent, the solution pH is considered as a crucial parameter in the adsorption phenomena. The reaction was carried out at pH levels ranging from 2 to 12. The obtained results are shown in Fig. 7.

Fig. 7 illustrates that the MB removal rate rises as a function of pH. This can be explained by the fact that, at low pH levels and below pHpzc, the adsorbent's surface is surrounded by H_3O^+ ions, which hinder the interaction between MB ions (a cationic pollutant) and the adsorbent's active sites. [83]. When pH exceeds pHpzc, more MB cations were adsorbed via attractive electrostatic attraction [84]. The maximum values of removal rate were observed at pH 9 and 12 with a yield of 96 % and 58 % for OP and PP, respectively. In the case of orange peels, a slight decrease in the elimination yield has been observed at pH > 9, which can be explained by the phenomenon of ion exchange, or MB precipitation,

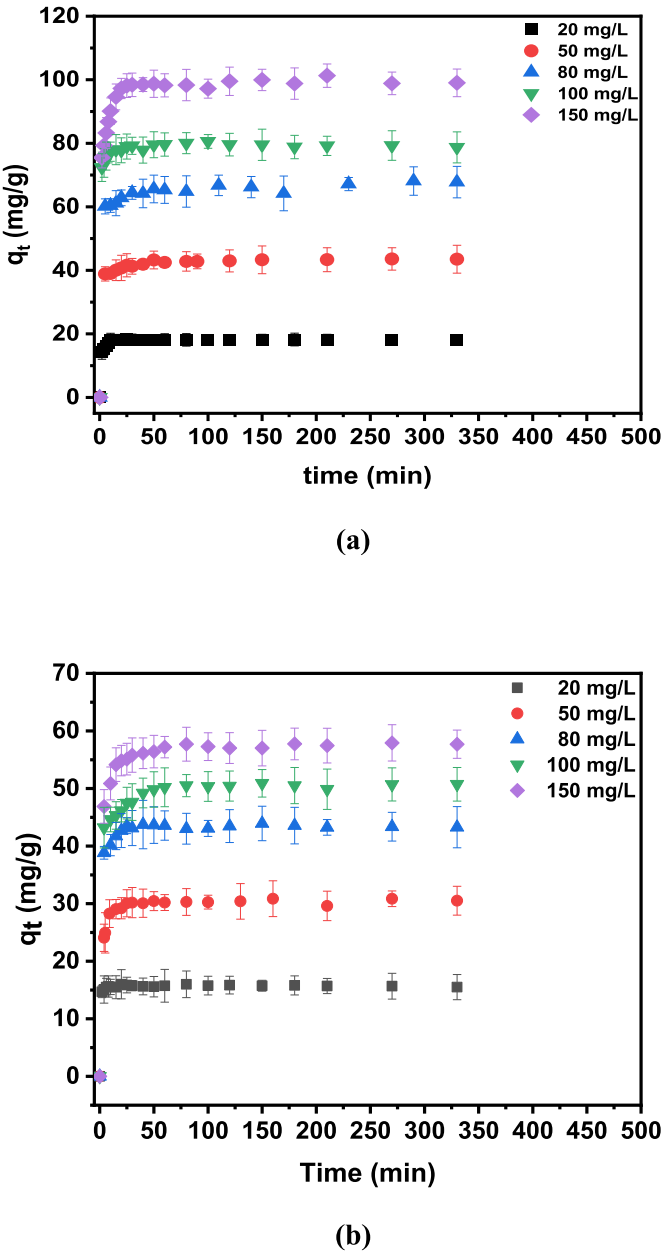

Fig. 5. Effect of contact time on the amount of MB adsorbed on OP (a) and PP (b) (pH = 7 ± 0.5, T = 25 °C ± 5, adsorbent dosage = 1 g/L, C_0 (MB) = 100 mg/l).

leading to a lower removal at higher pH [84].

3.5. Effect of particle size

Adsorption experiments were conducted from 100 to 600 μm to investigate the effect of particle size on methylene blue adsorption onto OP and PP. The obtained results are illustrated in Fig. 8.

Fig. 8 shows the removal efficiency of MB as a function of the adsorbents' particle size. The smaller particle size of an adsorbent provides a larger and more accessible surface, which leads to more significant yield of adsorption at equilibrium [85]. The best results were observed for particle sizes under 100 μm, as shown in the two histograms. However, for particle sizes exceeding 1000 μm, the removal efficiency significantly decreased to 69 % for OP and 31 % for PP.

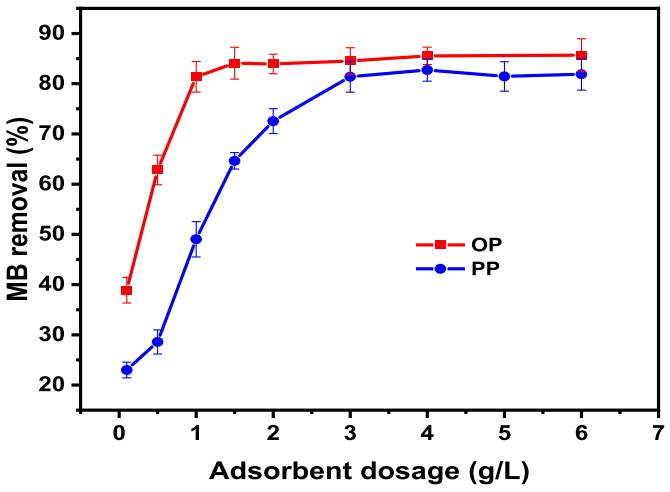

Fig. 6. Effect of biosorbents dosage on the MB removal. (pH = 7 ± 0.5, T = 25 °C ± 5, time = 180 min, C_0 (MB) = 100 mg/l).

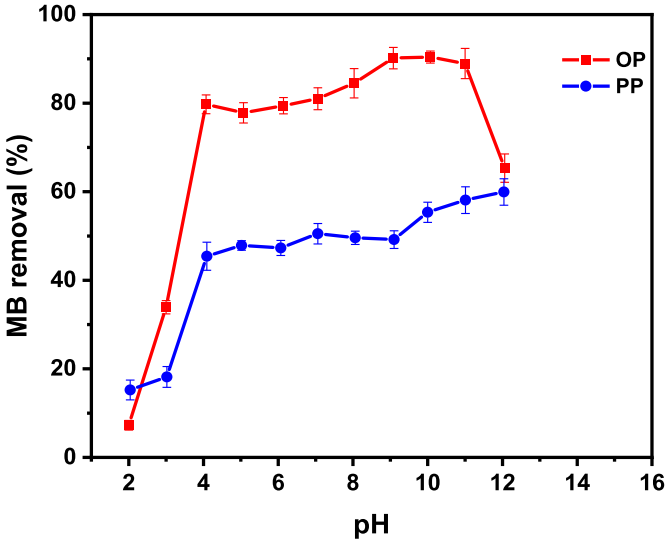

Fig. 7. Effect of pH on the adsorption of MB on orange peels OP and potato peels PP (T = 25 °C ± 5, adsorbent dosage = 1 g/L, time = 180 min, C_0 (MB) = 100 mg/l). (For interpretation of the references to color in this figure legend, the reader is referred to the Web version of this article.)

3.6. Effect of temperature

Adsorption experiments of MB onto OP and PL were carried out at 20, 30, 40, and 50 °C to observe the impact of temperature as shown in Fig. 9.

Fig. 9 illustrates the MB removal rate evolution as a function of temperature variation. The Figure shows that the best yield removal of adsorption occurs at a temperature of 20 °C with a yield of 81 % for OP and 53 % for PP. Increasing the temperature reduces the adsorbent's efficiency. This happens as the adsorption forces between the active sites and the adsorbed species weaken, possibly due to the deterioration of the adsorbent's active sites. The decrease in MB removal with rising temperature suggests that the adsorption process is likely exothermic [86].

3.7. Modeling of the adsorption kinetics

Modeling aims to align experimental data with theoretical models, providing insights into the adsorption mechanism and identifying key

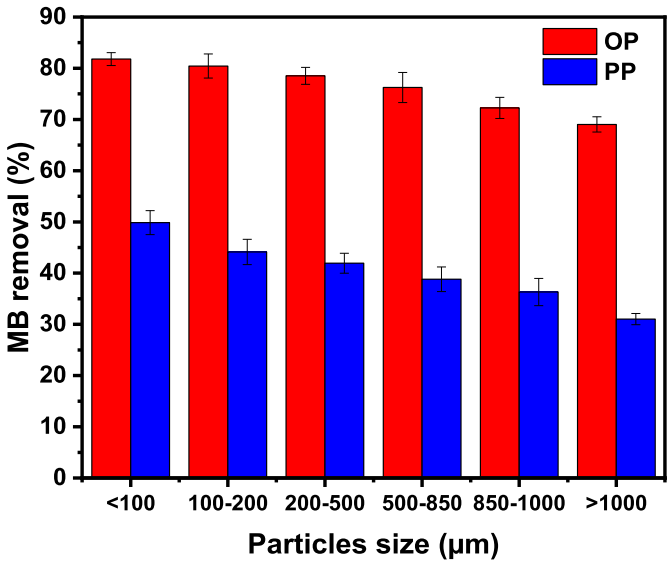

Fig. 8. Effect of particle size on the adsorption of MB on OP and PP. (pH = 7 ± 0.5, T = 25 °C ± 5, adsorbent dosage = 1 g/L, time = 180 min, C_0 (MB) = 100 mg/l).

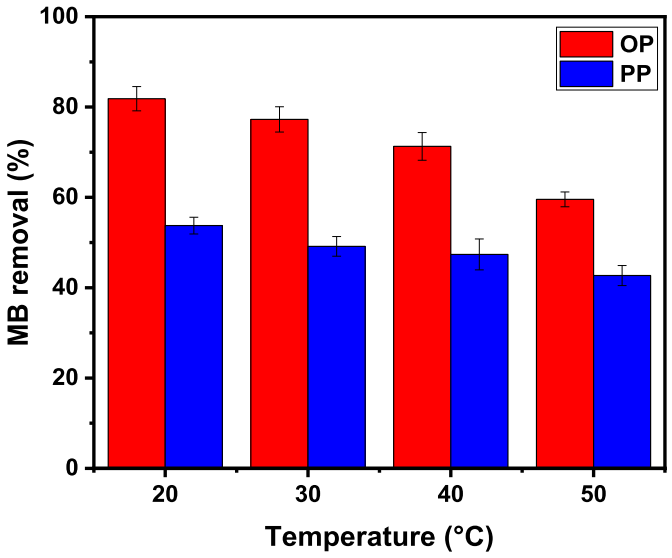

Fig. 9. Effect of temperature on the adsorption of MB on OP and PP (pH = 7 ± 0.5, time = 180 min, adsorbent dosage = 1 g/L, C_0 (MB) = 100 mg/l).

parameters influenced by physical or chemical processes [84]. The non-linear pseudo-first order (PFO) model, the pseudo-second order (PSO) model, and the intra-particle diffusion model were assessed in order to study the kinetic of solid-liquid interactions. The corresponding equations are listed in Table 3 [45,87].

Fig. 10 shows the fitting of the PFO and PSO kinetic models to the experimental data, and Table 4 provides the resulting kinetic parameters. The results show that for both adsorbents, the pseudo second-order model is better than the pseudo first-order model, since the PSO showed a high correlation coefficient ($R^2 > 0.99$). The amounts of adsorbed material determined experimentally were highly correlated with the q_{ecal} determined with the PSO model. This is confirmed by the graphical plots, which show a better alignment of the PSO curves with the theoretical results (Fig. 10). Although the R^2 values from the PSO model are higher than those from the PFO model, the R^2 values for the PFO model are still noteworthy, especially for the PP adsorbent. The amounts adsorbed calculated using the PFO model are closely match the

experimental values. This suggests that the PFO models can be effectively applied to describe the adsorption kinetics of methylene blue on OP and PP. These results indicate that the adsorption process of methylene blue on orange and potato peels may be influenced by both physisorption and chemisorption mechanisms. Similar conclusions were drawn by Jasri et al. [18] in their work on methylene blue adsorption on activated carbon derived from agricultural waste, including oil palm fronds (OPF) and palm kernel shells (PKS), using microwave-assisted K_2CO_3 activation.

Table 5 presents the computed kinetic parameters of the intra-particle model, while Fig. 11 depicts its fit to the experimental data, showing two distinct stages represented by two linear segments. According to Zamouche et al. [86], the first stage represented external diffusion, and the second one, intra-particle diffusion. When the fitted linear relationship plot crosses the origin, intra-particle diffusion is regarded as the rate-determining step. [88]. However, intra-particle diffusion is not the only rate-limiting process in this study, as the fitted lines do not go through the origin.

3.8. Adsorption isotherms

The phenomena of adsorption are typically explained in terms of their isothermal behavior. The equilibrium between the liquid and solid phases significantly affects the performance of the adsorbent. This equilibrium determines the maximum adsorption capacity that can be achieved under the operating conditions. In addition, the adsorption isotherms help to identify the type of adsorption that is likely to occur. They are obtained by plotting qe against Ce, where qe and Ce are the amount of dye adsorbed per gram of adsorbent and the equilibrium dye concentration, respectively. The adsorption of MB has been investigated using Langmuir and Freundlich. Table 6 presents the computed parameters, and Fig. 12 shows the model's fits to the experimental data.

The modeling results of the adsorption isotherms showed that the best results for both of OP and PP were obtained with the Langmuir model with values of $R^2 > 0.99$ (0.991 for OP, and 0.995 For PP). The Langmuir isotherm, with maximum adsorption capacities of 111.05 mg/g for OP and 71.66 mg/g for PP, provides a more accurate description of MB adsorption on these materials. This suggests that adsorption occurs as a monolayer on a homogeneous surface, with no interactions between the adsorbed molecules [89]. The results confirm that OP exhibits a higher MB adsorption efficiency than PP.

Based on the values of the Langmuir parameter K_L ($0<K_L<1$), MB is typically absorbed by the OP and PP [90]. In order to confirm whether the modelling using Langmuir equation of MB adsorption on OP and PP is favorable, a dimensionless constant named separation factor (R_L), given by equation (7), was calculated. The isotherm is favorable when $0 < R_L < 1$, unfavorable when $R_L > 1$, linear when $R_L = 1$, or irreversible when $R_L = 0$ [82,91].

$$R_L = \frac{1}{1 + K_L.C_0} \tag{7}$$

Where C_0 (mg/L) is the initial concentration of dye. The obtained results showed a R_L values of 0.05 for the OP adsorbent and 0.12 for the PP adsorbent, indicating that the adsorption process is favorable.

Table 3
Adsorption kinetics and isotherms models.

	Model	Equation	Parameters
Adsorption kinetics	Pseudo-first-order model	$q_t = q_e(1 - e^{-K_1 t})$	K_1: the pseudo-first-order kinetic rate constant (min^{-1})
	1. Pseudo-second-order model	$q_t = \frac{q_e^2 K_2 t}{1 + q_e k_2 t}$	K_2: the pseudo-second-order kinetic rate constant ($g{\cdot}mg^{-1}\ min^{-1}$)
	2. Intra-particle diffusion model	$q_t = K_p t^{1/2} + C$	K_p: intra-particle diffusion rate constant ($mg{\cdot}g^{-1}\ min^{-1/2}$)
			C a constant related to the boundary layer thickness ($mg{\cdot}g^{-1}$).
Adsorption isotherms	Langmuir model	$q_e = \frac{q_m K_L C_e}{1 + K_L C_e}$	K_L: Langmuir adsorption constant (L/mg) q_{max}: maximum MB adsorption capacity (mg/g)
	Freundlich model	$q_e = K_F.Ce^{1/n}$	K_F: Freundlich constant related to adsorption capacity [(mg/g)/(mg/L)^n] n: adsorption intensity constant

3.9. Study of the thermodynamic parameters

The study of the temperature effect showed that increasing the temperature from 20 to 50 °C leads to a decrease in the amounts of MB dye adsorbed on both adsorbents. The study of thermodynamic parameters provides insight into the nature and feasibility of adsorption processes. These parameters help to determine whether the process is endothermic or exothermic, to assess changes in randomness, and to evaluate its spontaneity [92]. The thermodynamic parameters of adsorption include the change in Gibbs free energy (ΔG^0, kJ/mol), the change in enthalpy (ΔH^0, kJ/mol), and the change in entropy (ΔS^0, kJ/mol. K). The relation between these parameters is given by equation (8) [93].

$$\Delta G^\circ = -RT.\mathrm{Ln}\ K_e^\circ = \Delta H^\circ - T\Delta S^\circ \tag{8}$$

Where T is the absolute adsorption temperature (K), and R is the gas constant (8.314 J/mol·K). K_e° is the thermodynamic equilibrium constant (dimensionless). The Van't Hoff equation was reformulated into its nonlinear form, as represented by the following equation

$$\mathrm{Ln}\ K_e^\circ = \frac{\Delta S^\circ}{R} - \frac{\Delta H^\circ}{RT} \tag{9}$$

As the Langmuir isotherm model exhibited the best fit for the experimental equilibrium data, the calculation of the thermodynamic equilibrium constant K_e° is based on the Langmuir adsorption constant (K_L) [87,93]. Given that K_L is expressed in L/mg, it must first be made dimensionless before being applied in the Van't Hoff equation. The calculation then follows the equations detailed below

$$K_e^\circ = \frac{K_L\left(\frac{L}{mol}\right) \times [\mathrm{Adsorbate}]^\circ\left(\frac{mol}{L}\right)}{\gamma_{MB}} \tag{10}$$

$$K_e^\circ = \frac{1000.\ K_L.M_{adsorbate}\ .[\mathrm{Adsorbate}]^\circ}{\gamma_{MB}} \tag{11}$$

Where γ_{MB} is the coefficient of activity (dimensionless) which is considered unitary, particularly in the context of very diluted adsorbate solutions. $M_{adsorbate}$ is the molar molecular weight of MB (319.85 g/mol). [Adsorbate]° is the standard concentration of the adsorbate (1 mol/L) [93–95].

Plotting $\ln(K_e^\circ)$ as a function of 1/T allows the determination of the values of ΔH^0 and ΔS^0 from the slope and the intercept of the Van't Hoff equation (equation (9)). ΔG° is calculated at different temperatures using equation (8) [96]. When the adsorption efficiency increases with temperature ($\Delta H^\circ > 0$), the process is endothermic; otherwise, it is exothermic [97]. The change in Gibbs free energy is a crucial factor in determining the degree of spontaneity of the adsorption process; the process will proceed favorably and spontaneously at a given temperature if ΔG° has a negative value [98]. Furthermore, the magnitude and sign of ΔS° help to indicate whether the organization of the adsorbate at the solid/solution interface during the adsorption process becomes less random ($\Delta S^\circ < 0$) or more random ($\Delta S^\circ > 0$) [98,99]. The obtained results are summarized in Table 7.

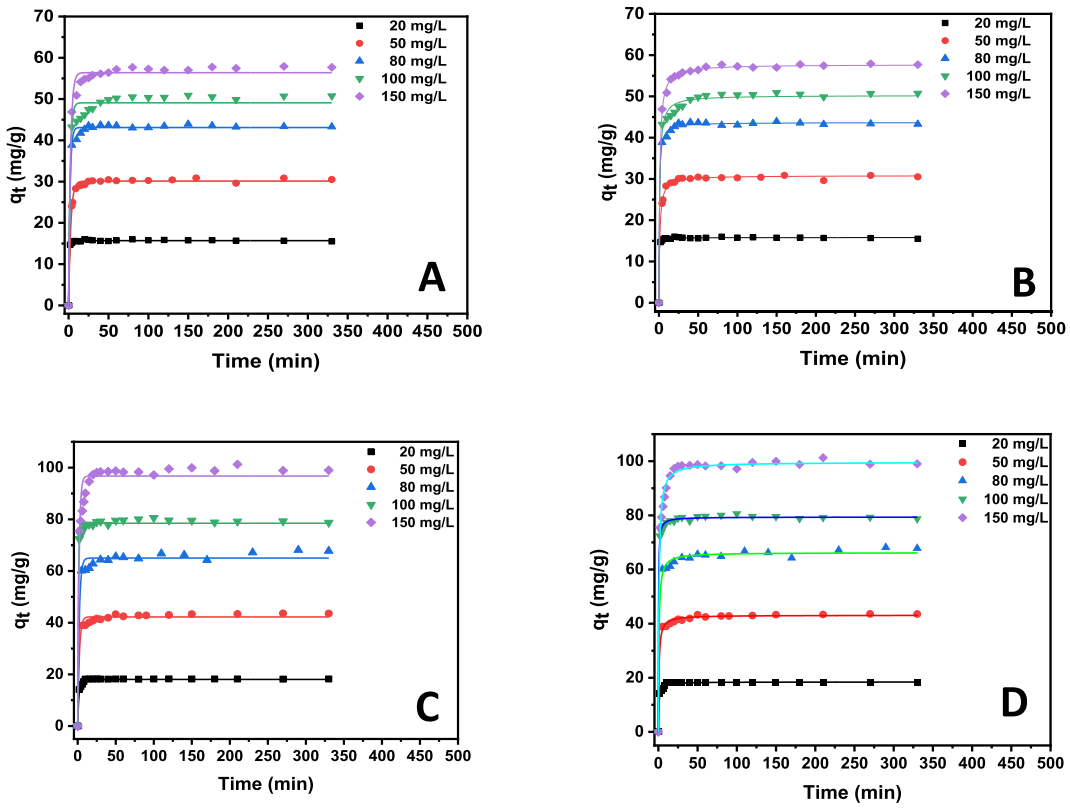

Fig. 10. Adsorption kinetic models (A) PFO kinetic model for Potato peels adsorbent, (B) PSO kinetic model for Potato peels adsorbent, (C) PFO kinetic model for Orange peels adsorbent, (D) PSO kinetic model for Orange peels adsorbent (pH = 7 ± 0.5, time = 180 min, adsorbent dosage = 1 g/L, T = 25 °C ± 5, C_0 (MB) = 100 mg/L). (For interpretation of the references to color in this figure legend, the reader is referred to the Web version of this article.)

Table 4
PFO and PSO adsorption parameters of MB dye adsorption onto OP and PP adsorbents.

			Pseudo-first order kinetic			Pseudo-second order kinetic		
	C_0 (mg.L^{-1})	qe_{exp} (mg.g^{-1})	qe_{cal} (mg.g^{-1})	K_1 (min^{-1})	R^2	qe_{cal} (mg.g^{-1})	K_2 (g·mg^{-1} min^{-1})	R^2
Orange peels (OP)	**20**	**18.75**	**18.03**	**0.631**	**0.980**	**18.43**	**0.085**	**0.994**
	50	**45.21**	**42.24**	**0.474**	**0.985**	**43.10**	**0.031**	**0.996**
	80	**66.74**	**65.02**	**0.487**	**0.984**	**66.22**	**0.021**	**0.993**
	100	**78.49**	**75.95**	**0.799**	**0.975**	**77.894**	**0.019**	**0.993**
	150	**98.54**	**96.74**	**0.573**	**0.952**	**99.61**	**0.011**	**0.991**
Potato peels (PP)	**20**	**14.86**	**15.686**	**1.364**	**0.997**	**15.791**	**0.430**	**0.996**
	50	**31.94**	**30.115**	**0.372**	**0.994**	**30.812**	**0.030**	**0.997**
	80	**46.00**	**41.129**	**0.489**	**0.982**	**42.013**	**0.028**	**0.995**
	100	**50.20**	**49.085**	**0.509**	**0.973**	**50.260**	**0.022**	**0.990**
	150	**57.03**	**56.390**	**0.420**	**0.986**	**57.740**	**0.017**	**0.998**

Table 5
Kinetic parameters for the adsorption of MB on OP and PP at various intra-particle diffusion concentrations.

	Intra-particle diffusion model						
		First stage			Second stage		
	C_0 (mg/L)	K_{P1} (mg.g^{-1} min$^{-1/2}$)	C_1 (mg.g^{-1})	R^2	K_{P2} (mg.g^{-1} min$^{-1/2}$)	C_2 (mg.g^{-1})	R^2
Orange peels (OP)	**20**	**2.294**	**10.730**	**0.990**	**0.020**	**18.029**	**0.963**
	50	**0.903**	**36.594**	**0.947**	**0.106**	**41.859**	**0.941**
	80	**1.208**	**57.043**	**0.942**	**0.464**	**60.303**	**0.894**
	100	**0.835**	**74.596**	**0.932**	**0.224**	**77.090**	**0.935**
	150	**7.460**	**65.157**	**0.988**	**0.586**	**94.958**	**0.921**
Potato peels (PP)	**20**	**0.680**	**13.752**	**0.976**	**0.074**	**15.332**	**0.952**
	50	**4.244**	**15.526**	**0.999**	**0.072**	**29.691**	**0.959**
	80	**1.614**	**35.428**	**0.988**	**0.069**	**42.671**	**0.983**
	100	**1.390**	**40.219**	**0.985**	**0.115**	**49.102**	**0.949**
	150	**3.384**	**40.268**	**0.977**	**0.145**	**56.174**	**0.984**

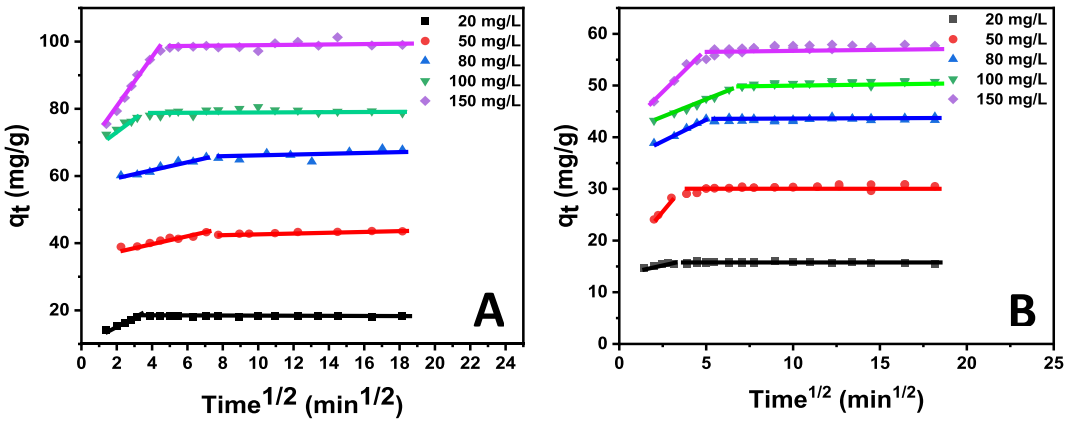

Fig. 11. Adsorption kinetics of MB on OP: intra-particle diffusion (pH = 6.87, T = 25 °C ± 5).

Table 6
Isotherm parameters for MB adsorption onto OP and PP adsorbents.

Isotherm Model	Parameters values	
	OP	PP
Langmuir	q_{max} = 111.05 mg/g K_L = 0.128 L/mg R^2 = 0.991	q_{max} = 71.66 mg/g K_L = 0.048 L/mg R^2 = 0.995
Freundlich	K_F = 28.193 [(mg/g)/(mg/L)^n] 1/n = 0.301 R^2 = 0.954	K_F = 11.816 [(mg/g)/(mg/L)^n] 1/n = 0.350 R^2 = 0.943

The obtained results show that the values of Gibbs free energy of adsorption (ΔG°) are negative for the adsorption of MB dye on both adsorbents. This indicates the spontaneity of the adsorption process. The results also show that the negative values of ΔG° decrease with increasing temperature, suggesting that the adsorption process is more favorable at lower temperatures [100]. Furthermore, the negative values for ΔH° indicate that the adsorption process is exothermic [101]. The ΔH° values are less than 40 kJ/mol for both adsorbents, suggesting that the adsorption is mainly physical in nature [102]. The positive values of ΔS° suggest the increased randomness at the solid-liquid interface during the adsorption of MB onto OP and PP adsorbents [91].

3.10. Adsorption mechanism

Agricultural residues are mainly constituted of cellulose, hemicellulose and lignin, rich in various functional groups. These components promote dye fixation through various interaction mechanisms [103].

In order to explain the reaction mechanisms potentially involved in the adsorption of methylene blue (MB) on the two adsorbents (OP and PP), it is essential to analyze the adsorbent characterization results as well as the thermodynamic parameters. FTIR analysis revealed the presence of various functional groups on the surface of both adsorbents, an observation confirmed by Boehm titration. In addition, a change in the intensities of certain characteristic peaks (-*O*-H groups, C═C, C–H and -C-O bonds) was observed after MB adsorption, attesting to the involvement of carboxyl and phenolic groups in the dye binding process on the adsorbent surfaces [104]. Furthermore, the study of thermodynamic parameters demonstrated that MB adsorption on OP and PP is a physisorption. This phenomenon relies mainly on electrostatic interactions, the formation of hydrogen bonds and n-π interactions [105]. Adsorption tests were carried out at a solution pH above pHpzc, resulting in a negative charge on adsorption sites on the adsorbent surface. This negative charge promotes electrostatic interaction with methylene blue molecules, facilitating their attachment to the adsorbent surface [106]. The study of pH effect showed that the dye solution's pH had a major impact on the uptake of MB. The adsorption of MB rises in tandem with the pH. The electrostatic interactions between the dye particles and the biosorbent may account for the increase in MB uptake in alkaline circumstances [104]. Hydrogen bonding can also take place between the nitrogen atoms of MB molecules (acting as hydrogen acceptors) and the oxygen-containing functional groups (-OH or –COOH) present on the surface of both adsorbents (acting as hydrogen donors) [107]. This interaction is supported by the FTIR spectra of MB adsorption on OP and PP (MB-PP and MB-OP), which show a reduction in the intensity of the –OH stretching vibration around 3400 cm^{-1}, indicating the formation of hydrogen bonds. The n-π interaction involves electron donor atoms on the biosorbent surface, and aromatic rings of MB, which

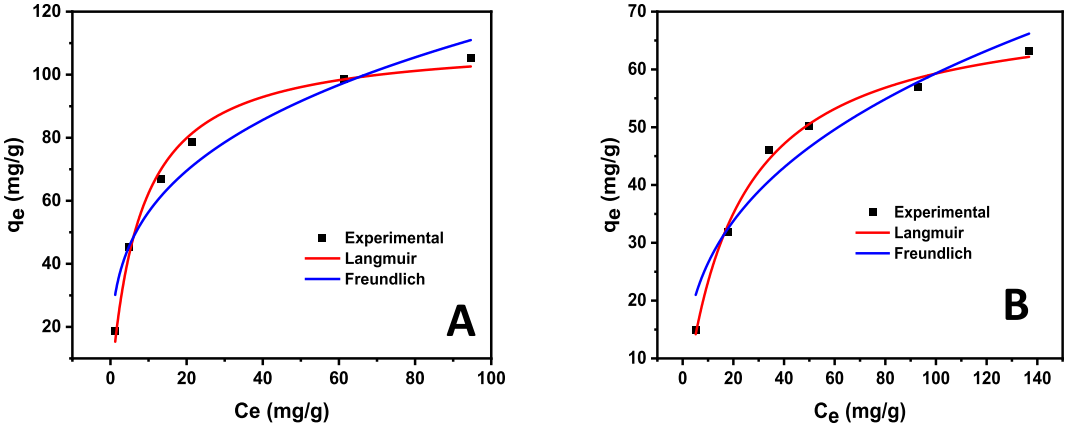

Fig. 12. Adsorption isotherm of MB on OP (A) and PP (B).

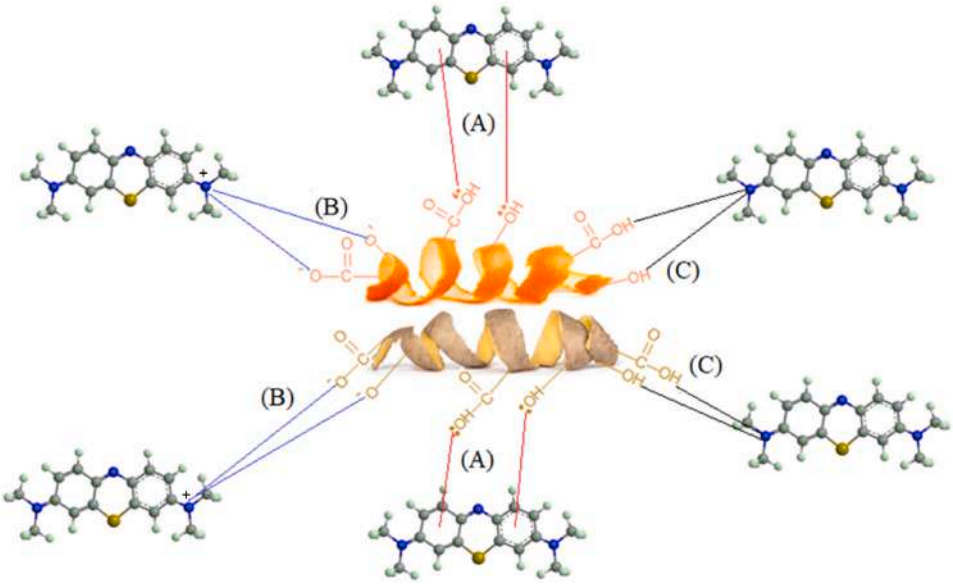

Fig. 13. MB adsorption mechanism on OP and PP adsorbents; (A) n-π interaction, (B) electrostatic interactions, (C) hydrogen bonding.

Table 7
Thermodynamic parameters of the MB adsorption on the OP and PP adsorbents.

Adsorbent	T (K)	$K_e^{\circ} \times 10^3$	ΔG° (kJ/mol)	ΔH° (kJ/mol)	ΔS° (kJ/mol.K)	R^2
OP	293	30.603	−25.037	−24,714	0,001	0.981
	303	19.527	−25.048			
	313	14.713	−25.059			
	323	11.857	−25.070			
PP	293	15.474	−23.553	−21,444	0,007	0.996
	303	12.170	−23.624			
	313	9.097	−23.696			
	323	6.864	−23.768			

act as electron acceptors [105,108]. The following figure resume the three possible mechanisms of the MB adsorption on the surface of orange and potato peels.

3.11. Coupling support vector machine with coupled with boosting and improved Grey Wolf Optimizer algorithm

In this study, an SVM-Boosting model was used to predict the amount of MB adsorbent on OP and PP adsorbents. MB adsorption data was collected and used to train the model. The database was normalized and divided into training and validation sets. The Gaussian kernel function was chosen for the SVM model due to its ability to solve non-linear problems and handle outliers. The parameters of the Gaussian kernel function were optimized using the IGWO algorithm (SVM-Boosting-IGWO). The Boosting process was performed to train a strong model by focusing on errors [53,54]. By combining these methods, the SVM-Boosting-IGWO model offers a promising approach to predict the amount of MB adsorbent on OP and PP adsorbents. From the beginning, MB adsorption data was used to train and validate the model exclusively using SVM_IGWO. The results are presented in Table 8 (see Fig. 13).

The results from Table 8 indicate that the initial model achieved excellent performance during the training phase, with R = 0.99997 and R^2 = 0.99994 (Fig. 14a). This suggests a strong correlation and an excellent ability of the model to explain the variation in the training data. Additionally, the negligible RMSE indicates that the model's predictions are very close to the actual values during the training phase. However, during the validation phase, the model's performance deteriorates. The R drops to 0.9366 (Fig. 14b), indicating an unreliable correlation between the predictions and the actual values in the validation set. Similarly, the R^2 decreases to 0.8772 (Table 8), meaning that the model explains approximately 87.72 % of the variation in the validation data. Finally, the RMSE of 9.3396 (Table 8) indicates some dispersion of predictions compared to the actual values in the validation set. These results suggest that the initial model may tend to overfit the training data, meaning it adapts too precisely to the specific data of the training set, resulting in a decrease in performance when faced with new data (validation set). It's possible that the model learned specific characteristics from the training data that do not generalize well to the validation data. It would be wise to explore regularization techniques or other methods to improve the model's performance during the validation phase, ensuring better generalization and prediction of unknown data.

For this purpose, the Boosting process was performed 30 times to train a strong model by focusing on errors. The results of the Boosting model are presented in Table T1 (see supplementary material), indicating the R, R^2, and RMSE values from the validation phase.

The results demonstrate a significant improvement in the evaluation metrics (R, R^2, and RMSE) at each stage of the Boosting process. This indicates that the initial model (SVM_IGWO) was strengthened and refined through iterations, leading to an overall better performance. The correlation coefficient R increased substantially at each Boosting stage, ranging from 0.9366 for the initial model to 1 for the 30th iteration (Fig. 15). This suggests that the model's predictions are increasingly closely linked to the actual values as Boosting progresses. Similarly, the determination coefficient R^2 increased significantly with each iteration, eventually reaching a value close to 1 (0.99999). This means that the improved model explains a large portion of the variance in the MB adsorption data, indicating its better fit to the data (Fig. 15). As for the RMSE, it decreased significantly with each iteration, going from 9.3396 for the initial model to 0.00038 for the 30th iteration (Fig. 15). A lower RMSE indicates better accuracy of the model's predictions compared to the actual values, suggesting that the improved model is capable of

Table 8
Performances of the first model (SVM_IGWO).

	R/R^2			RMSE		
	Train	VAL	ALL	Train	VAL	ALL
SVM_IGWO	0.99997 0.99994	0.93664 0.8772	0.98157 0.9911	0.002	9.3396	5.4361

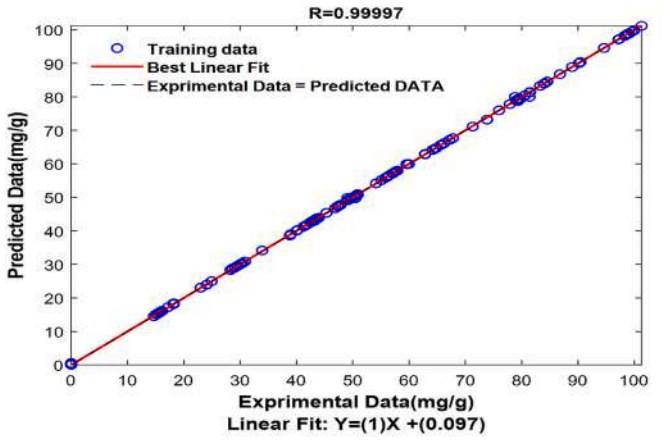

(a)

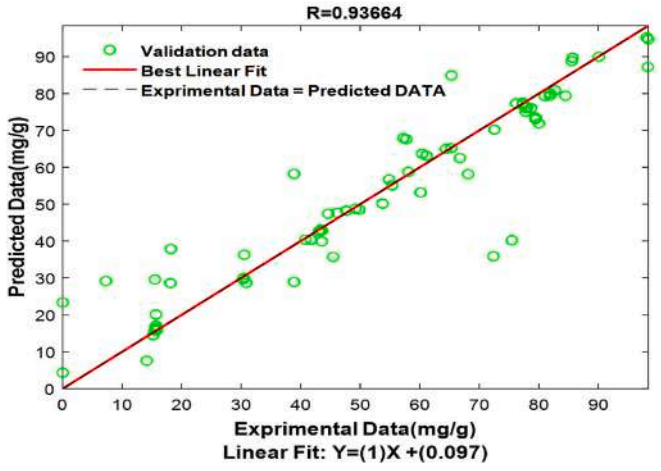

(b)

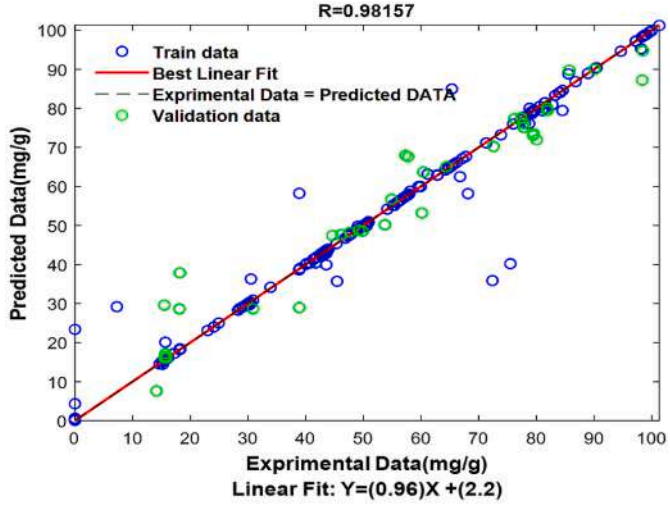

(c)

Fig. 14. Relationship between the experimental and the SVM_IGWO model predicted values: (a) training, (b) validation and (c) all data.

making more precise predictions. The Boosting process significantly enhanced the performance of the initial model (SVM-IGWO).

The results indicate a stronger correlation, better explanatory power, and more accurate predictions for the MB adsorption quantity. This demonstrates the effectiveness of Boosting in strengthening the model and achieving better results. However, we observed that after the 12th iteration of Boosting, the error became negligible. By plotting the surface of the RMSE and R according to the number of Boosting, as well as the evolution of the RMSE according to the number of Boosting, a significant decreasing trend was observed. As the number of Boosting iterations increased, the RMSE decreased until the 12th iteration (Fig. 16a). After this iteration, the error became negligible (Fig. 16b). This finding led us to select the model from the 12th Boosting as our final model.

Indeed, at this stage, the RMSE has reached a very low value, indicating excellent prediction accuracy for our model. Additionally, both R and R^2 have also reached their maximum value of 1, highlighting the robustness and suitability of the model to the MB adsorption data. The use of the Boosting process clearly improved the performance of the initial model based on SVM-IGWO, progressively reducing the RMSE error. After selecting the model, the database was once again predicted through the three phases, and the obtained results are represented in the following Table.

The results from Table 9 confirm that the selection of the model from the 12th Boosting is justified by this significant decrease in error, demonstrating the model's ability to capture complex relationships between the input variables and the MB adsorption response. Overall, our study highlights the effectiveness of the Boosting process in improving the performance of the initial model. The model from the 12th Boosting exhibits high precision in predicting MB adsorption, making it suitable for use in future applications. The results from the model derived from the 12th Boosting have also been visually presented in Figure F1 (see supplementary material).

3.11.1. Analysis of model residuals

A residual analysis was carried out to assess the performance of the model from the 12th Boosting by comparing the experimental values with model predictions [63]. The relationship between the experimental results and the model predictions was initially shown by a plot (Fig. 17a). This allows us to assess the degree of agreement between the two data sets. A good match between the projected and experimental values would be indicated by the points being near the reference line. After analysis, a significant connection was found between the experimental results and the model's 12th Boosting predictions (Fig. 17a). The

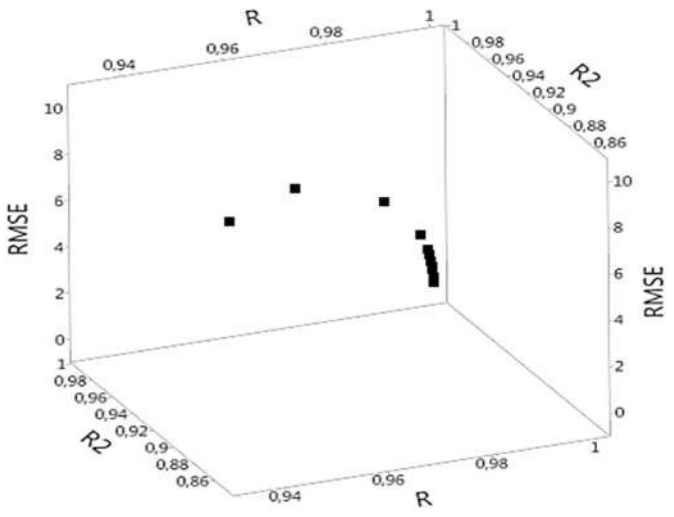

Fig. 15. Analysis of the performance of the SVM-IGWO-Boosting model by Surface of the R and R^2 according to RMSE.

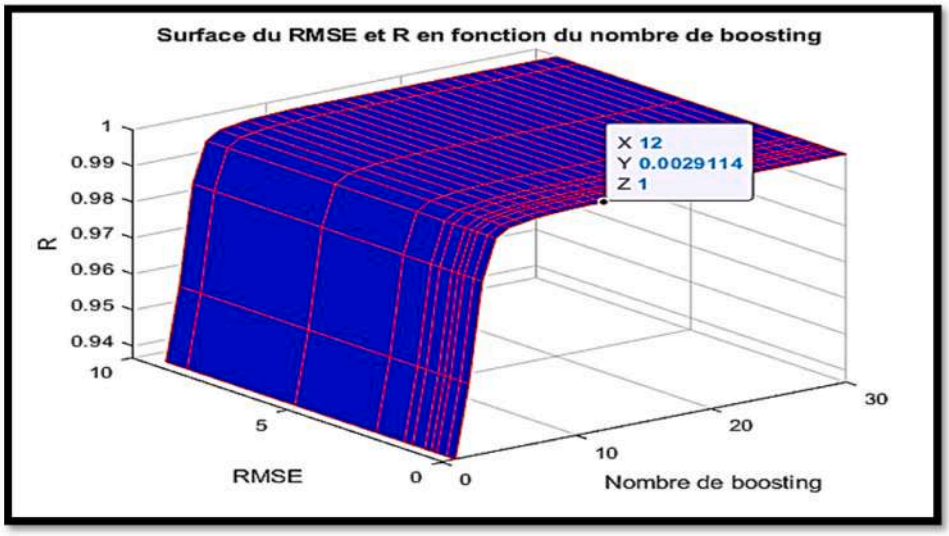

(a)

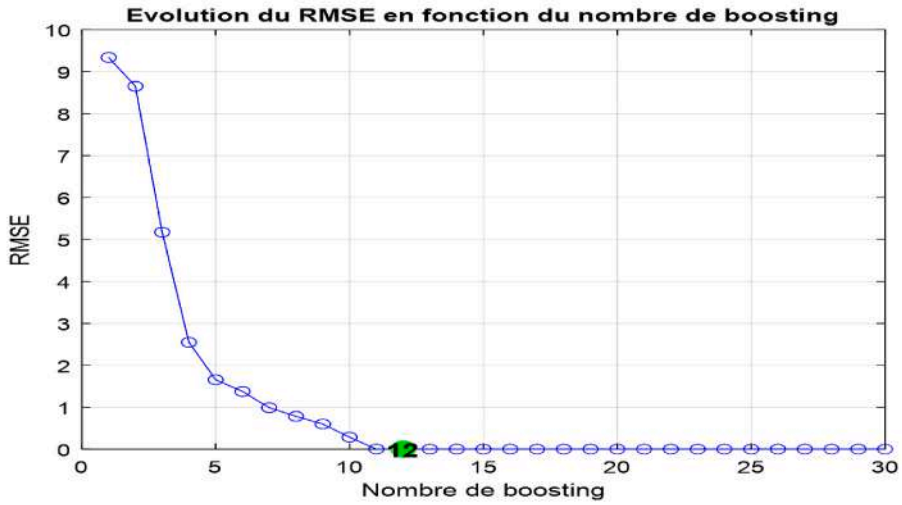

(b)

Fig. 16. Analysis of the performance of the SVM-IGWO-Boosting model: (a) Surface of the RMSE and R according to the number of Boosting and (b) Evolution of the RMSE according to the number of Boosting.

Table 9
Performances of the 12th Boosting of model SVM_IGWO_Boosting.

	R/R^2			RMSE		
	Train	VAL	ALL	Train	VAL	ALL
SVM_IGWO_Boosting	0.99998 0.99996	1 1	0.99999 0.99999	0.0023	0.0021	0.0022

points are all overlapping, suggesting that the model is capable of accurately reproducing the experimental values. In addition to this visual analysis, a histogram of the frequency of residuals was also plotted (Fig. 17b). This helps to gain a better understanding of the error distribution between the experimental values and the model predictions [12]. In a well-fitted model, a distribution of residuals centered around zero is expected (Fig. 17a), indicating a good balance between predictions and experimental observations. The frequency histogram confirmed the previous observation, showing a distribution of residuals centered around zero (Fig. 17a) [52]. This confirms that the model from the 12th Boosting is capable of capturing the variations in the experimental data accurately, with an overall low error.

The residual analysis conducted on the model from the 12th Boosting demonstrates its satisfactory performance in predicting the

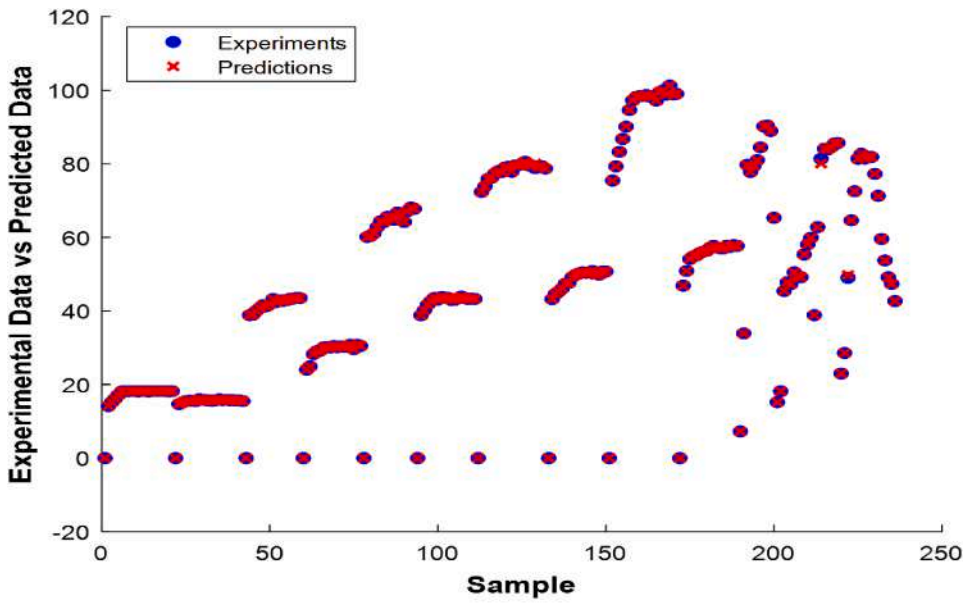

(a)

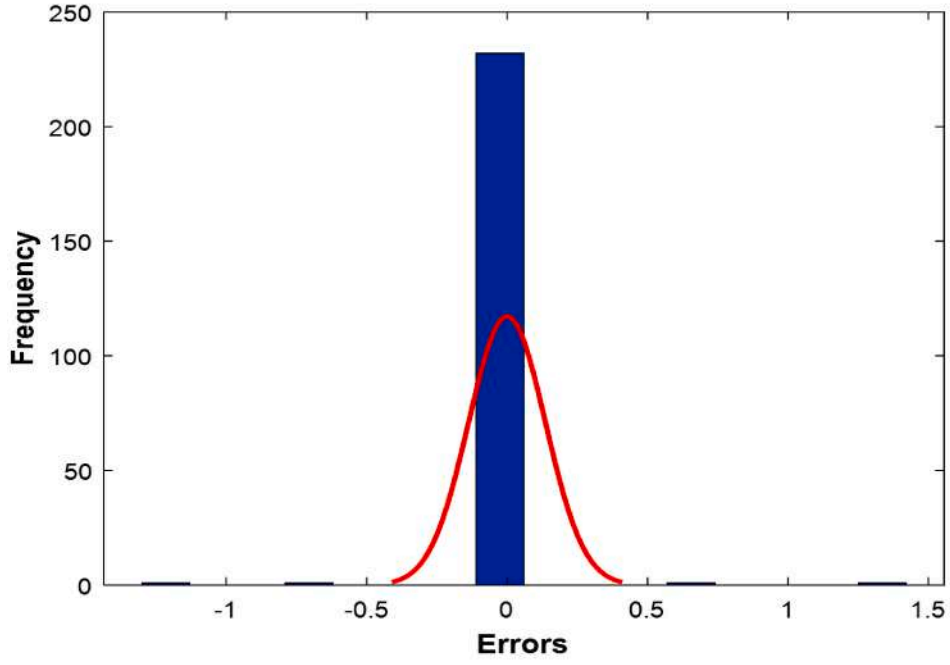

(b)

Fig. 17. Residuals relating to the model established by SVM_IGWO_Boosting: (a) Relationship between experimental data and the predicted data of samples, and (b) Histogram distribution of errors.

experimental values. The results and frequency histogram confirm the adequacy of the model to the observed data. These findings enhance our confidence in the use of the model from the 12th Boosting for future applications.

3.11.2. Model performance test

An independent test was conducted to evaluate the model's performance using a dataset not utilized for training and validation. Several metrics were calculated to assess the model's accuracy once it was applied to this new dataset.

The obtained results are very promising, with both R and R^2 equal to 1 (Figure F2, supplementary material), indicating a perfect correlation between predicted model values and the actual test dataset values. This means that the model is able to accurately capture the variations and trends present in these unseen data. Furthermore, the obtained RMSE is only 0.002, confirming the very low prediction error of the model. Such a low RMSE indicates that the model's predictions are extremely close to the actual values of the test dataset. These results strongly suggest that

the model is capable of generalizing to new data and maintaining its accuracy even on unseen observations. This strengthens confidence in the model's performance and paves the way for its utilization in real-world applications where reliability and precision are crucial.

3.11.3. Optimization and validation of the optimum conditions

To obtain and to validate the optimal inputs for each adsorbent, the Improved Grey Wolf Optimization (IGWO) algorithm was utilized [54]. The objective was to determine the values of input parameters that maximize the adsorption efficiency of each adsorbent. Initially, input parameter ranges were defined for each adsorbent, such as the initial concentration of the adsorbate, pH, temperature, contact time, and adsorbent mass. Subsequently, the IGWO algorithm was employed to optimize these parameters.

The IGWO algorithm is an optimization technique inspired by the social behavior of grey wolves [54]. It mimics the social hierarchy of wolves to find the best possible solutions. The algorithm was implemented by iteratively updating the positions of wolves throughout the search space In each iteration, the alpha, beta, and delta wolves, representing the best solutions found so far, were identified [54]. The positions of wolves were updated using search and movement operations to effectively explore the search space. The IGWO algorithm gradually converges towards optimal solutions by adjusting the positions of wolves [54]. Once the optimal parameters were obtained, experimental validation was performed. The optimum parameters for each adsorbent were used in adsorption trials. Then, the experimental data were compared to the values predicted by the IGWO algorithm. These results are shown in Table 10.

The results in Table 10 demonstrated excellent agreement between the experimental data and the predicted values, with errors not exceeding 0.16 mg/g. This confirms that the optimal inputs obtained using the IGWO algorithm effectively optimize the adsorption efficiency of each adsorbent.

For the OP adsorbent, the optimal values of input variables are as follows: X1 = 179.4573 min, X2 = 3.4077, X3 = 149.9999, X4 = 9.3401, and X5 = 20 °C. These optimal conditions yielded a predicted value of MB adsorption capacity of 111.7524 mg/g, while the experimental value was 111.5983 mg/g. The error between the predicted and experimental values was only 0.1541 mg/g. This indicates that the IGWO model is capable of accurately capturing the adsorption behavior of MB by orange peels, enabling reliable prediction of adsorption capacity from the provided optimal conditions. In the case of the OP adsorbent, it is significant to notice that the maximum adsorption capacity values derived from the Langmuir model and the IGWO optimization using the SVM-IGWO-Boosting model are the same. This can be interpreted as a confirmation of the validity of the Langmuir model in describing the adsorption behavior of the OP adsorbent. The Langmuir model is a widely used empirical model for describing solute adsorption on heterogeneous surfaces. It assumes multilayer adsorption with variable adsorption energy, which can explain the obtained maximum adsorption capacity.

The IGWO optimization using the SVM-IGWO-Boosting model determines the optimal values of input variables to maximize the predicted adsorption capacity. In the case of the OP adsorbent, it appears that the obtained optimal values correspond to the maximum adsorption capacity predicted by the Langmuir model. This implies that the Langmuir model is a good descriptor of the adsorption behavior of the OP adsorbent, and the optimal values obtained through IGWO optimization are consistent with this model. However, it is necessary to note that the Langmuir model is a simplification of reality, and other more complex models may provide a better description of the adsorption system.

Table 10
Comparison between actual and predicted responses at optimum conditions.

OP	
IGWO: X1 = 179.4573 min, X2 = 3.4077, X3 = 149.9999, X4 = 9.3401, and X5 = 20 °C	
MB uptake (mg/g). Predicted values	111.7524
MB uptake (mg/g). Experimental values	111.5983
Error (mg/g)	0.1541
PP	
IGWO: X1 = 179.8890 min, X2 = 4.6971, X3 = 149.9999, X4 = 8.3319, and X5 = 20 °C	
MB uptake (mg/g). Predicted values	96.6753
MB uptake (mg/g). Experimental values	96.7385
Error (mg/g)	0.0632

For the PP adsorbent, the optimal values of input variables are as follows: X1 = 179.8890 min, X2 = 4.6971, X3 = 149.9999, X4 = 8.3319, and X5 = 20 °C. The predicted value of MB adsorption capacity under these optimal conditions is 96.6753 mg/g, while the experimental value is 96.7385 mg/g. The error between the predicted and experimental values is only 0.0632 mg/g. These results confirm the effectiveness of the IGWO model in accurately predicting the adsorption capacity of MB by potato peels. When using the Langmuir model to estimate the maximum adsorption capacity of the PP adsorbent, a value of 71.66 mg/g was obtained. However, by using the IGWO algorithm to optimize the input variable values based on the SVM-IGWO-Boosting model, a new optimal value (96.6753 mg/g) was found. This difference between the previous experimental value and the predicted optimal value can be explained by the combined effect of input variable optimization and the improved performance of the SVM-IGWO-Boosting model.

The IGWO algorithm searches for the optimal values of input variables that better fit the model to the experimental data, resulting in a better estimation of the MB adsorption capacity for the PP adsorbent. On the other hand, the Langmuir model, although well-fitted to the data as indicated by an R^2 value close to 1, remains a mathematical model that does not consider all the experimental parameters involved in the adsorption process. This may demonstrate a limitation of these purely theoretical models compared to the experimental results, especially when the calculated result is lower compared to the empirically obtained result. Therefore, it is noteworthy that the Langmuir model is an empirical model that suggests that adsorption occurs as a monolayer on a homogeneous surface, with no interactions between the adsorbed molecules. However, this simplified model may not capture all the complex aspects of the adsorption process on the PP adsorbent. Hence, the results obtained by this model may deviate from the actual experimental values. This highlights the advantage of using artificial intelligence techniques such as the IGWO algorithm combined with the SVM-IGWO-Boosting model. These more advanced methods can consider a larger number of variables and relationships between variables, enabling more accurate predictions and optimization of experimental conditions.

The obtained results demonstrate that the IGWO algorithm combined with the SVM-IGWO-Boosting model exhibits high performance in predicting the MB adsorption capacities for the OP and PP adsorbents. The predicted values are in close agreement with the experimental values, indicating the reliability and precision of the developed model.

Using the IGWO algorithm to obtain and validate the optimal inputs for each adsorbent has demonstrated the effectiveness of the developed model. The IGWO algorithm efficiently explores the search space and finds optimal combinations of parameters that maximize adsorption efficiency. By mimicking the social behavior of grey wolves, the algorithm converges towards high-quality solutions. Experimental validation has confirmed the performance of the developed model. The experimental data showed excellent agreement with the values predicted by the IGWO algorithm, indicating that the identified optimal inputs achieve high levels of adsorption efficiency.

Through the use of the IGWO algorithm, we can optimize the performance of each adsorbent by precisely adjusting the input parameters. This paves the way for more efficient utilization of adsorbents in adsorption applications, such as wastewater treatment or air purification. The approach based on the use of sustainable agricultural materials like orange peels and potato peels offers significant advantages in terms

of resource sustainability and availability. It represents a promising alternative to conventional methods of wastewater treatment. These encouraging results open up avenues for further research and applications of the IGWO algorithm in other areas of adsorption and wastewater treatment. The use of this algorithm could enable the optimization of treatment processes for different classes of pollutants and adsorbents, thereby contributing to more efficient and sustainable solutions for water depollution.

3.12. Interface for optimization and prediction

In addition to our research, we have developed a user-friendly application in the form of a MATLAB interface to optimize the efficiency of our approach using the IGWO algorithm and the SVM-IGWO-Boosting model. With this application (Fig. 18), users can specify the ideal parameters for MB adsorption by orange peel and potato peel-based adsorbents, including contact time, pH, temperature, and adsorbent quantity. Furthermore, this application provides also the ability to predict the adsorbent amount required to achieve a desired depollution level. This innovative approach optimizes resource utilization and facilitates the implementation of this wastewater treatment technique on a large scale. The application serves as a valuable tool for researchers and professionals in the field of water depollution, offering a practical and efficient solution to assess and optimize the performance of pollutant adsorption in aqueous solutions.

3.13. Comparison of the performances of OP and PP bio-adsorbents with other adsorbents

The maximum methylene blue adsorption amounts achieved on the investigated unmodified bio-adsorbents after the optimization and prediction of the adsorption amount with the SVM_IGWO_Boosting model were found to be 111.75 and 96.67 mg/g for orange and potato peels, respectively.

The results obtained in this study are comparable to those reported in the literature (Table 11). Both this study and previous research have demonstrated the effectiveness of unmodified bio-adsorbents derived from potato and orange peels. In particular, orange peels have consistently demonstrated excellent performance in the removal of methylene blue, confirming their effectiveness as a low-cost and cost-effective alternative for the treatment of methylene blue-contaminated water.

4. Conclusion

The aim of this study was to assess the potential of using orange peels (OP) and potato peels (PP), as agricultural waste, for effective removal the methylene blue from aqueous solutions. The adsorption isotherms followed the Langmuir model, with maximum adsorption capacities of 111.05 mg/g and 71.66 mg/g. The pseudo-second order model, showing a significant correlation ($R^2 > 0.99$), best explained the MB adsorption kinetics on PP and OP. The thermodynamic study demonstrated the spontaneous and the exothermic nature of the adsorption process, which is mainly physical in nature, governed by electrostatic attraction, hydrogen bonding, and n-π interactions. Additionally, by combining Support Vector Machine (SVM), Boosting, and the Improved Grey Wolf Optimizer (IGWO) algorithm, a novel predictive model was created. With perfect correlation and low prediction error, the SVM-IGWO-Boosting model performed remarkably well in predicting MB adsorption. The input parameters for the adsorbents were successfully optimized by the IGWO optimization approach, resulting excellent agreement between experimental and projected values. Furthermore, this modeling showed that OP had a maximum adsorption capacity of 111.75 mg/g compared to 96.67 mg/g for PP using IGWO, making them more effective at removing MB than PP.

The use of OP and PP as agricultural waste offers an effective and sustainable alternative for the MB removal. The SVM-IGWO-Boosting predictive model, along with the IGWO optimization approach, shows great potential for improving the efficiency of MB adsorption. These results open up interesting possibilities for practical applications requiring accurate and reliable predictions.

CRediT authorship contribution statement

Nasma Bouchelkia: Writing – review & editing, Writing – original draft, Software, Resources, Methodology, Data curation, Conceptualization. **Hichem Tahraoui:** Writing – original draft, Software, Resources, Investigation, Conceptualization. **Kheira Benazouz:** Writing – original draft, Methodology. **Amal Mameri:** Formal analysis, Data curation, Conceptualization. **Reguia Boudraa:** Software, Formal analysis. **Hamza Moussa:** Software, Methodology, Investigation. **Nadia Hamri:** Writing – original draft, Investigation. **Ryma Merdoud:** Writing – review & editing, Writing – original draft, Conceptualization. **Hayet Belkacemi:** Visualization, Validation, Supervision, Project administration, Conceptualization. **Abdelhalim Zoukel:** Visualization, Validation, Supervision,

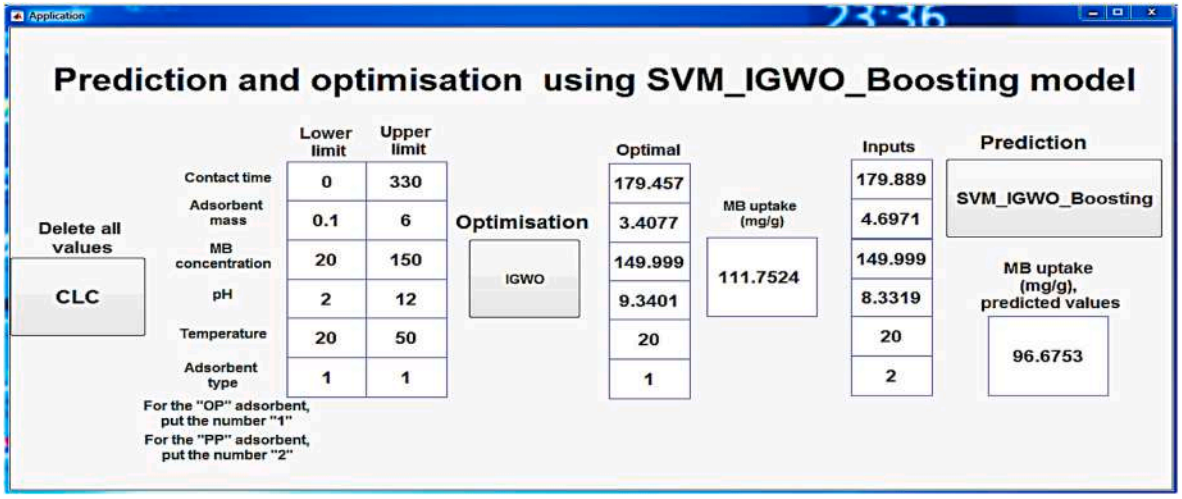

Fig. 18. MATLAB Interface: Optimization and prediction of the adsorption quantity with SVM_IGWO_Boosting model.

Table 11
Comparison of the MB adsorption capacity on unmodified bio-adsorbents.

Adsorbent	Experimental conditions	Maximum MB adsorption capacity (mg/g)	Reference
Orange peels	[a]bd: 0.8 g/L, pH: 6.5, T: ambient, C_{MB}: 15 mg/L, t: 1 h speed: 200 rpm	10.96	[32]
Potato peel residue from starch extraction process	[a]bd: 8 g/L, pH:6.5, T: 25 °C, C_{MB}: 30 mg/L, t: 140 min speed: 200 rpm	25.00	[35]
Longkong Fruit Peels	[a]bd: 1 g/L, pH:7, T: 30 °C, C_{MB}: 50 mg/L, t: 205min, speed: 180 rpm	45.85	[109]
Ziziphus lotus fruit peels	[a]bd: 1 g/L, pH:7, T: 25 °C, C_{MB}: 100 mg/L, t: 120min	59.07	[110]
Avocado kernels seeds	[a]bd: 1 g/L, pH:7, T: 25 °C, C_{MB}: 100 mg/L, t: 120min	66.04	[110]
Potato peels	[a]bd: 4.70 g/L, pH:8.33, T: 20 °C, C_{MB}: 150 mg/L, t: 180 min, speed: 200 rpm	96.67	This study
Potato peels	[a]bd: 2 g/L, pH:7, T: 30 °C, C_{MB}: 100 mg/L, t: 10 min.	97.08	[33]
Potato peels	[a]bd: 2 g/L, pH:6.2, T: 25 °C, C_{MB}: 100 mg/L, t: 300 min, speed: 200 rpm	105.26	[111]
Potato peels	[a]bd: 1 g/L, pH:6, T: 25 °C, C_{MB}: 300 mg/L, t: 24h, speed: 12 rpm	107.2	[103]
Orange peels	[a]bd: 3.41 g/L, pH:9.34, T: 20 °C, C_{MB}: 150 mg/L, t: 179.45 min, speed: 200 rpm	111.75	This study
Banana peels	[a]bd: 1 g/L, pH of the solution, T: 22 °C, C_{MB}: 200 mg/L, t: 40 min.	111.11	[112]
fava bean peels	[a]bd: 5 g/L, pH:5.8, T:27 °C, C_{MB}: 50 mg/L, t: 24h	140.00	[7]
Cucumber peels	[a]bd: 1 g/L, pH:6, T: 25 °C, C_{MB}: 300 mg/L, t: 24h, speed: 12 rpm	179.9	[103]
watermelon	[a]bd: 0.6 g/L, pH:5.6, T: 30 °C, C_{MB}: 100 mg/L, t: 180min, speed: 120 rpm	188.68	[113]
dragon fruit (Hylocereus polyrhizus) peels	[a]bd: 0.6 g/L, pH:5.6, T: 30 °C, C_{MB}: 100 mg/L, t: 180min, speed: 120 rpm	192.31	[114]
Almond peels	[a]bd: 1 g/L, pH of the solution (4.2–5), T: 25 °C, C_{MB}: 300 mg/L, speed: 400 rpm	208.82	[115]
Banana peels	[a]bd: 1 g/L, pH:6, T: 25 °C, C_{MB}: 300 mg/L, t: 24h, speed: 12 rpm	211.9	[103]
Orange peels	[a]bd: 1 g/L, pH of the solution (4.2–5), T: 25 °C, C_{MB}: 300 mg/L, speed: 400 rpm	218.82	[115]
Orange peels	[a]bd: 1 g/L, pH:7, T:27 °C, C_{MB}: 250 mg/L, t: 24h, speed: 200 rpm	250.6	[34]

[a] bd: biosorbent dosage.

Software, Resources. **Abdeltif Amrane:** Validation, Supervision, Project administration. **Mohammed Kebir:** Writing – original draft, Software, Resources. **Lotfi Mouni:** Visualization, Validation, Supervision, Project administration, Formal analysis.

Declaration of competing interest

The authors declare that they have no known competing financial interests or personal relationships that could have appeared to influence the work reported in this paper.

Appendix A. Supplementary data

Supplementary data to this article can be found online at https://doi.org/10.1016/j.chemolab.2025.105377.

Data availability

No data was used for the research described in the article.

References

[1] S.A. Yasin, J.A. Abbas, M.M. Ali, I.A. Saeed, I.H. Ahmed, Methylene blue photocatalytic degradation by TiO_2 nanoparticles supported on PET nanofibres, Mater. Today Proc. 20 (2020) 482–487.

[2] B.H. Díez, C.A. Torres, S.P. Gaudêncio, Actinomycete-derived pigments: a path toward sustainable industrial colorants, Mar. Drugs 23 (2025) 39.

[3] A. Imessaoudene, S. Cheikh, J.-C. Bollinger, L. Belkhiri, A. Tiri, A. Bouzaza, A. El Jery, A. Assadi, A. Amrane, L. Mouni, Zeolite waste characterization and use as low-cost, ecofriendly, and sustainable material for malachite green and methylene blue dyes removal: box–behnken design, kinetics, and thermodynamics, Appl. Sci. 12 (2022) 7587.

[4] H. Karaer, I. Kaya, Synthesis, characterization of magnetic chitosan/active charcoal composite and using at the adsorption of methylene blue and reactive blue4, Microporous Mesoporous Mater. 232 (2016) 26–38.

[5] M.A. Hassaan, A. El Nemr, A. Hassaan, Health and environmental impacts of dyes: mini review, American Journal of Environmental Science and Engineering 1 (2017) 64–67.

[6] S. Abu-Melha, Adsorption optimization of VNi-layered double hydroxide encapsulated with chitosan and carboxymethyl cellulose for rhodamine B dye removal from aqueous solutions: adsorption isotherm, kinetics, and thermodynamics, Appl. Organomet. Chem. 39 (2025) e7937.

[7] O.S. Bayomie, H. Kandeel, T. Shoeib, H. Yang, N. Youssef, M.M. El-Sayed, Novel approach for effective removal of methylene blue dye from water using fava bean peel waste, Sci. Rep. 10 (2020) 7824.

[8] M. Kurniasih, N.H. Aprilita, R. Roto, M. Mudasir, Modification of coal fly ash for high capacity adsorption of methylene blue, Case Studies in Chemical and Environmental Engineering (2025) 101101.

[9] L. Mouni, L. Belkhiri, J.-C. Bollinger, A. Bouzaza, A. Assadi, A. Tirri, F. Dahmoune, K. Madani, H. Remini, Removal of Methylene Blue from aqueous solutions by adsorption on Kaolin: kinetic and equilibrium studies, Appl. Clay Sci. 153 (2018) 38–45.

[10] K. Madi, D. Chebli, H. Ait Youcef, H. Tahraoui, A. Bouguettoucha, M. Kebir, J. Zhang, A. Amrane, Green fabrication of ZnO nanoparticles and ZnO/rGO nanocomposites from Algerian date syrup extract: synthesis, characterization, and augmented photocatalytic efficiency in methylene blue degradation, Catalysts 14 (2024) 62.

[11] A. Hadadi, A. Imessaoudene, J.-C. Bollinger, S. Cheikh, A.A. Assadi, A. Amrane, M. Kebir, L. Mouni, Parametrical study for the effective removal of mordant black 11 from synthetic solutions: moringa oleifera seeds' extracts versus alum, Water 14 (2022) 4109.

[12] A. Hadadi, A. Imessaoudene, J.-C. Bollinger, A. Bouzaza, A. Amrane, H. Tahraoui, L. Mouni, Aleppo pine seeds (Pinus halepensis Mill.) as a promising novel green coagulant for the removal of Congo red dye: optimization via machine learning algorithm, J. Environ. Manag. 331 (2023) 117286.

[13] H. Tahraoui, S. Toumi, M. Boudoukhani, N. Touzout, A.N.E.H. Sid, A. Amrane, A.-E. Belhadj, M. Hadjadj, Y. Laichi, M. Aboumustapha, Evaluating the effectiveness of coagulation–flocculation treatment using aluminum sulfate on a polluted surface water source: a year-long study, Water 16 (2024) 400.

[14] S. Mechati, M. Zamouche, H. Tahraoui, O. Filali, S. Mazouz, I.N.E. Bouledjemer, S. Toumi, Z. Triki, A. Amrane, M. Kebir, Modeling and optimization of hybrid Fenton and ultrasound process for crystal violet degradation using AI techniques, Water 15 (2023) 4274.

[15] M. Kebir, I.-K. Benramdhan, N. Nasrallah, H. Tahraoui, N. Baït, H. Benaissa, R. Ameraoui, J. Zhang, A.A. Assadi, L. Mouni, Surface response modeling of homogeneous photo Fenton Fe (III) and Fe (II) complex for sunlight degradation and mineralization of food dye, Catal. Commun. 183 (2023) 106780.

[16] D. Balarak, T.J. Al-Musawi, I.A. Mohammed, H. Abasizadeh, The eradication of reactive black 5 dye liquid wastes using Azolla filiculoides aquatic fern as a good and an economical biosorption agent, SN Appl. Sci. 2 (2020) 1015.

[17] T.A. Yousef, U.K. Sahu, A.H. Jawad, N.N. Abd Malek, O. Al Duaij, Z.A. Alothman, Fruit peel-based mesoporous activated carbon via microwave assisted K_2CO_3 activation: Box Behnken design and desirability function for methylene blue dye adsorption, Int. J. Phytoremediation 25 (2023) 1142–1154.

[18] K. Jasri, A.S. Abdulhameed, A.H. Jawad, Z.A. Alothman, T.A. Yousef, O. Al Duaij, Mesoporous activated carbon produced from mixed wastes of oil palm frond and palm kernel shell using microwave radiation-assisted K_2CO_3 activation for methylene blue dye removal: optimization by response surface methodology, Diam. Relat. Mater. 131 (2023) 109581.

[19] A. Bhardwaj, M. Bansal, K. Wilson, S. Gupta, M. Dhanawat, Lignocellulose biosorbents: unlocking the potential for sustainable environmental cleanup, Int. J. Biol. Macromol. 294 (2025) 139497.

[20] A.S. Franca, L.S. Oliveira, M.E. Ferreira, Kinetics and equilibrium studies of methylene blue adsorption by spent coffee grounds, Desalination 249 (2009) 267–272.
[21] G. Crini, G. Torri, E. Lichtfouse, G.Z. Kyzas, L.D. Wilson, N. Morin-Crini, Dye removal by biosorption using cross-linked chitosan-based hydrogels, Environ. Chem. Lett. 17 (2019) 1645–1666.
[22] A. Díaz, J. Marrero, G. Cabrera, O. Coto, J. Gómez, Optimization of nickel and cobalt biosorption by native Serratia marcescens strains isolated from serpentine deposits using response surface methodology, Environ. Monit. Assess. 194 (2022) 167.
[23] N.S. Razali, A.S. Abdulhameed, A.H. Jawad, Z.A. Alothman, T.A. Yousef, O.K. Al-Duaij, N.S. Alsaiari, High-surface-area-activated carbon derived from mango peels and seeds wastes via microwave-induced $ZnCl_2$ activation for adsorption of methylene blue dye molecules: statistical optimization and mechanism, Molecules 27 (2022) 6947.
[24] P. Praipipat, P. Ngamsurach, K. Bunchu, V. Lekwaree, P. Srirat, P. Chaiphumee, J. Noisri, T. Aeamsa-ard, Comparative performance of fruit peel materials for methylene blue dye adsorption, Int. J. Environ. Sci. Technol. (2024) 1–20.
[25] E.B. Onuk, B. Isik, Adsorptive removal of toxic methylene blue and crystal violet dyes from aqueous solutions using Prunus spinosa: isotherm, kinetic, thermodynamic, and error analysis, Biomass Conversion and Biorefinery (2025) 1–18.
[26] W.A.S. El-Dein, Z.A. Mahdi, H.R. Lotfy, A comprehensive study on pomegranate (Punicagranatum) peels as a low-cost biosorbent: adsorption mechanisms, application, regeneration, and cost analysis, Environ. Monit. Assess. 197 (2025) 229.
[27] A.S. Semercioöz, F. Göğüş, A. Ļelekli, H. Bozkurt, Development of carbonaceous material from grapefruit peel with microwave implemented-low temperature hydrothermal carbonization technique for the adsorption of Cu (II), J. Clean. Prod. 165 (2017) 599–610.
[28] D. Ramutshatsha-Makhwedzha, A. Mavhungu, M.L. Moropeng, R. Mbaya, Activated carbon derived from waste orange and lemon peels for the adsorption of methyl orange and methylene blue dyes from wastewater, Heliyon 8 (2022) e09930.
[29] A.A. Al-Gheethi, M.S. Mohd Salleh, E.A. Noman, R.M.S.R. Mohamed, R. Crane, R. Hamdan, M. Naushad, Cephalexin adsorption by acidic pretreated jackfruit adsorbent: a deep learning prediction model study, Water 14 (2022) 2243.
[30] S. Adunphatcharaphon, A. Petchkongkaew, D. Greco, V. D'Ascanio, W. Visessanguan, G. Avantaggiato, The effectiveness of durian peel as a multi-mycotoxin adsorbent, Toxins 12 (2020) 108.
[31] L.B. Lim, N. Priyantha, S.A. Latip, Y.C. Lu, A.H. Mahadi, Converting Hylocereus undatus (white dragon fruit) peel waste into a useful potential adsorbent for the removal of toxic Congo red dye, Desalination Water Treat. 185 (2020) 307–317.
[32] A.D. Rosanti, Y. Kusumawati, F. Hidayat, A. Fadlan, A.R. Wardani, H. A. Anggraeni, Adsorption of methylene blue and methyl orange from aqueous solution using orange peel and CTAB-modified orange peel, Journal of the Turkish Chemical Society Section A: Chemistry 9 (2022) 237–246.
[33] K. Ben Jeddou, F. Bouaziz, F. Ben Taheur, O. Nouri-Ellouz, R. Ellouz-Ghorbel, S. Ellouz-Chaabouni, Adsorptive removal of direct red 80 and methylene blue from aqueous solution by potato peels: a comparison of anionic and cationic dyes, Water Sci. Technol. 83 (2021) 1384–1398.
[34] S. Giraldo, N.Y. Acelas, R. Ocampo-Pérez, E. Padilla-Ortega, E. Flórez, C. A. Franco, F.B. Cortés, A. Forgionny, Application of Orange Peel waste as adsorbent for methylene blue and Cd^{2+} simultaneous remediation, Molecules 27 (2022) 5105.
[35] A. Hadadi, A. Imessaoudene, J.-C. Bollinger, S. Cheikh, A. Manseri, L. Mouni, Dual valorization of potato peel (Solanum tuberosum) as a versatile and sustainable agricultural waste in both bioflocculation of eriochrome black T and biosorption of methylene blue, J. Polym. Environ. 23 (2023) 2983–2998.
[36] FAO, Agricultural production statistics 2010–2023, in: FAOSTAT Analytical Briefs, No. 96, FAO, Rome, 2024.
[37] B. Tadesse, S. Gebeyehu, L. Kirui, J. Maru, The contribution of potato to food security, income generation, employment, and the national economy of Ethiopia, research report, International potato center, CGIAR (2025).
[38] K. Açıkalın, Evaluation of orange and potato peels as an energy source: a comprehensive study on their pyrolysis characteristics and kinetics, Biomass Conversion and Biorefinery 12 (2022) 501–514.
[39] R. Kamboj, D. Ms, Orange peel extract enhanced sugar recovery and butanol production from potato peel by Clostridium acetobutylicum, Int. J. Green Energy 18 (2021) 987–997.
[40] N.A.M. Hanafi, A.S. Abdulhameed, A.H. Jawad, Z.A. Alothman, T.A. Yousef, O. Al Duaij, N.S. Alsaiari, Optimized removal process and tailored adsorption mechanism of crystal violet and methylene blue dyes by activated carbon derived from mixed orange peel and watermelon rind using microwave-induced $ZnCl_2$ activation, Biomass Conversion and Biorefinery 14 (2024) 28415–28427.
[41] M. Filipi, M. Milichovsk'y, Adsorption organic cationic dyes of oxycelluloses and linters, J. Encapsulation Adsorpt. Sci. 4 (2014) 1–7.
[42] A.K. Samanta, A. Konar, Dyeing of textiles with natural dyes, Natural dyes 3 (2011).
[43] A. Ogunlaja, I.N. Nwankwo, M.E. Omaliko, O.D. Olukanni, Biodegradation of methylene blue as an evidence of synthetic dyes mineralization during textile effluent biotreatment by Acinetobacter pittii, Environmental Processes 7 (2020) 931–947.
[44] S. Ali, H. Ijaz, M.U. Ahmad, Rukhma, N. Ullah, A. Sarwar, M.J. Khan, T. Aziz, A. shami, F. Al-Asmari, Photocatalytic removal of textile wastewater-originated methylene blue and malachite green dyes using spent black tea extract-coated silver nanoparticles, Sci. Rep. 15 (2025) 1851.
[45] N. Bouchelkia, H. Tahraoui, A. Amrane, H. Belkacemi, J.-C. Bollinger, A. Bouzaza, A. Zoukel, J. Zhang, L. Mouni, Jujube stones based highly efficient activated carbon for methylene blue adsorption: kinetics and isotherms modeling, thermodynamics and mechanism study, optimization via response surface methodology and machine learning approaches, Process Saf. Environ. Prot. 170 (2023) 513–535.
[46] S.K. Sharma, D.S. Verma, L.U. Khan, S. Kumar, S.B. Khan, Handbook of Materials Characterization, Springer International Publishing, 2018.
[47] H. Khan, A.S. Yerramilli, A. D'Oliveira, T.L. Alford, D.C. Boffito, G.S. Patience, Experimental methods in chemical engineering: X-ray diffraction spectroscopy—XRD, Can. J. Chem. Eng. 98 (2020) 1255–1266.
[48] A.A. Bunaciu, E.G. UdriŞTioiu, H.Y. Aboul-Enein, X-ray diffraction: instrumentation and applications, Crit. Rev. Anal. Chem. 45 (2015) 289–299.
[49] N. Bouchelkia, L. Mouni, L. Belkhiri, A. Bouzaza, J.-C. Bollinger, K. Madani, F. Dahmoune, Removal of lead (II) from water using activated carbon developed from jujube stones, a low-cost sorbent, Separ. Sci. Technol. 51 (2016) 1645–1653.
[50] S.A. Bakar Fatiatun, A. Mohamed, H.H. Kusuma, Muqoyyanah, R. Mohamat, V. V. Kumar, K. Ali, R. Nuryadi, M.N.A. Azis, High methylene blue adsorption efficiency of cellulose acetate-based electrospun nanofiber membranes modified with graphene oxide and zeolite, Int. J. Environ. Res. 19 (2025) 18.
[51] H. Tahraoui, A.-E. Belhadj, N. Moula, S. Bouranene, A. Amrane, Optimisation and prediction of the coagulant dose for the elimination of organic micropollutants based on turbidity, Kem. Ind. 70 (2021) 675–691.
[52] H. Tahraoui, A.-E. Belhadj, A. Amrane, E.H. Houssein, Predicting the concentration of sulfate using machine learning methods, Earth Science Informatics 15 (2022) 1023–1044.
[53] H. Tahraoui, A. Amrane, A.-E. Belhadj, J. Zhang, Modeling the organic matter of water using the decision tree coupled with bootstrap aggregated and least-squares boosting, Environ. Technol. Innovat. 27 (2022) 102419.
[54] A. Seyyedabbasi, F. Kiani, I-GWO and Ex-GWO: improved algorithms of the Grey Wolf Optimizer to solve global optimization problems, Eng. Comput. 37 (2021) 509–532.
[55] A. Bousselma, D. Abdessemed, H. Tahraoui, A. Amrane, Umjetna inteligencija i matematičko modeliranje kinetike sušenja prethodno obrađenih cjelovitih plodova marelice, Kemija u industriji: Časopis kemičara i kemijskih, inženjera Hrvatske 70 (2021) 651–667.
[56] M. Kebir, I. kahina Benramdhan, N. Noureddine, H. Tahraoui, B. Nadia, B. Houssine, A. Rachid, J. Zhang, A.A. Assadi, L. Mouni, Sunlight Degradation and Mineralization of Food Dye Photoinduced by Homogenous Photo Fenton Fe (III) and Fe (II)/Complex: Surface Response Modeling, 2023.
[57] M. Nedjhioui, N. Nasrallah, M. Kebir, H. Tahraoui, R. Bouallouche, A.A. Assadi, A. Amrane, B. Jaouadi, J. Zhang, L. Mouni, Designing an efficient surfactant–polymer–oil–electrolyte system: a multi-objective optimization study, Processes 11 (2023) 1314.
[58] H. Tahraoui, A.-E. Belhadj, A.-E. Hamitouche, M. Bouhedda, A. Amrane, Predicting the concentration of sulfate (SO_4^{2-}) in drinking water using artificial neural networks: a case study: Médéa-Algeria, Desalination Water Treat. 217 (2021) 181–194.
[59] H. Tahraoui, A.-E. Belhadj, A.-E. Hamitouche, Prediction of the bicarbonate amount in drinking water in the region of Médéa using artificial neural network modelling, Kem. Ind.: Časopis kemičara i kemijskih inženjera Hrvatske 69 (2020) 595–602.
[60] M.M. Yahoum, S. Toumi, S. Hentabli, H. Tahraoui, S. Lefnaoui, A. Hadjsadok, A. Amrane, M. Kebir, N. Moula, A.A. Assadi, Experimental analysis and neural network modeling of the rheological behavior of xanthan gum and its derivatives, Materials 16 (2023) 2565.
[61] M. Zamouche, H. Tahraoui, Z. Laggoun, S. Mechati, R. Chemchmi, M.I. Kanjal, A. Amrane, A. Hadadi, L. Mouni, Optimization and prediction of stability of emulsified liquid membrane (ELM): artificial neural network, Processes 11 (2023) 364.
[62] A. Guediri, A. Bouguettoucha, H. Tahraoui, D. Chebli, A. Amrane, J. Zhang, Thermodynamic study and the development of a support vector machine model for predicting adsorption behavior of orange peel-derived beads in wastewater treatment, J. Mol. Liq. 403 (2024) 124860.
[63] H. Tahraoui, A.-E. Belhadj, Z. Triki, N.R. Boudella, S. Seder, A. Amrane, J. Zhang, N. Moula, A. Tifoura, R. Ferhat, A. Bousselma, N. Mihoubi, Mixed coagulant-flocculant optimization for pharmaceutical effluent pretreatment using response surface methodology and Gaussian process regression, Process Saf. Environ. Prot. 169 (2022) 909–927.
[64] J.R. Njimou, V. Fai, M.T. Sieugaing, D. Nguenamadje, J. Godwin, O.B. Genola, G. B. Noumi, B.C. Tripathy, Hydrothermal synthesis of a nickel-oxide-infused orange peel nanobiocomposite for enhanced heavy metal removal from mining wastewater, Hybrid Advances 9 (2025) 100392.
[65] N.M. Mahmoodi, M. Taghizadeh, A. Taghizadeh, Mesoporous activated carbons of low-cost agricultural bio-wastes with high adsorption capacity: preparation and artificial neural network modeling of dye removal from single and multicomponent (binary and ternary) systems, J. Mol. Liq. 269 (2018) 217–228.
[66] J.S. Yaradoddi, N.R. Banapurmath, S.V. Ganachari, M.E.M. Soudagar, A. M. Sajjan, S. Kamat, M. Mujtaba, A.S. Shettar, A.E. Anqi, M.R. Safaei, Bio-based material from fruit waste of orange peel for industrial applications, J. Mater. Res. Technol. 17 (2022) 3186–3197.
[67] O. Üner, Ü. Geçgel, Y. Bayrak, Adsorption of methylene blue by an efficient activated carbon prepared from Citrullus lanatus rind: kinetic, isotherm,

thermodynamic, and mechanism analysis, Water, Air, Soil Pollut. 227 (2016) 247.
[68] A.H. Jawad, A.S. Abdulhameed, L.D. Wilson, S.S.A. Syed-Hassan, Z.A. Alothman, M.R. Khan, High surface area and mesoporous activated carbon from KOH-activated dragon fruit peels for methylene blue dye adsorption: optimization and mechanism study, Chin. J. Chem. Eng. 32 (2021) 281–290.
[69] A.C. Arampatzidou, E.A. Deliyanni, Comparison of activation media and pyrolysis temperature for activated carbons development by pyrolysis of potato peels for effective adsorption of endocrine disruptor bisphenol-A, J. Colloid Interface Sci. 466 (2016) 101–112.
[70] A.H. Jawad, N.N. Abd Malek, T. Khadiran, Z.A. Alothman, Z.M. Yaseen, Mesoporous high-surface-area activated carbon from biomass waste via microwave-assisted-H3PO4 activation for methylene blue dye adsorption: an optimized process, Diam. Relat. Mater. 128 (2022) 109288.
[71] D. Kibami, P. Chubaakum, K. Rao, S. Dipak, Preparation and characterization of activated carbon from Fagopyrum esculentum Moench by HNO3 and H3PO4 chemical activation, Chem. Sin. 5 (2014) 46–55.
[72] N. Bouchelkia, K. Benazouz, A. Mameri, L. Belkhiri, N. Hamri, H. Belkacemi, A. Zoukel, A. Amrane, F. Aoulmi, L. Mouni, Study and characterization of H_3PO_4 activated carbons prepared from jujube stones for the treatment of industrial textile effluents, Processes 11 (2023) 2694.
[73] Z. Bahnes, N. Benderdouche, S. Attouti, B. Bestani, L. Duclaux, L. Reinert, Preparation of a novel activated carbon from jujube stones (Ziziphus jujuba) for the removal of basic and acid dyes, Desalination Water Treat. 102 (2018) 312–325.
[74] C. Du, B. Liu, J. Hu, H. Li, Determination of iodine number of activated carbon by the method of ultraviolet–visible spectroscopy, Mater. Lett. 285 (2021) 129137.
[75] X. Yuan, S.-P. Zhuo, W. Xing, H.-Y. Cui, X.-D. Dai, X.-M. Liu, Z.-F. Yan, Aqueous dye adsorption on ordered mesoporous carbons, J. Colloid Interface Sci. 310 (2007) 83–89.
[76] K. Benazouz, N. Bouchelkia, A. Imessaoudene, J.-C. Bollinger, A. Amrane, A. A. Assadi, H. Zeghioud, L. Mouni, Efficient and low-cost water remediation for chitosan derived from shrimp waste, an ecofriendly material: kinetics modeling, response surface methodology optimization, and mechanism, Water 15 (2023) 3728.
[77] H. Thangappan, A. Valiya Parambathu, S. Joseph, Surface characterization and methylene blue adsorption studies on a mesoporous adsorbent from chemically modified Areca triandra palm shell, Desalination Water Treat. 57 (2016) 21118–21129.
[78] S. Altenor, B. Carene, E. Emmanuel, J. Lambert, J.-J. Ehrhardt, S. Gaspard, Adsorption studies of methylene blue and phenol onto vetiver roots activated carbon prepared by chemical activation, J. Hazard Mater. 165 (2009) 1029–1039.
[79] S. Farch, M.M. Yahoum, S. Toumi, H. Tahraoui, S. Lefnaoui, M. Kebir, M. Zamouche, A. Amrane, J. Zhang, A. Hadadi, Application of walnut shell biowaste as an inexpensive adsorbent for methylene blue dye: isotherms, kinetics, thermodynamics, and modeling, Separations 10 (2023) 60.
[80] F.-T. Zohra, S. Ahmed, M.Z. Alam, M. Nurnabi, N. Rahman, Bio-waste to environmental purifier: application of potato peel for acid red 73 adsorption from leather dyeing effluent, Water Resour. Ind. (2025) 100281.
[81] K. Bellir, M.B. Lehocine, A.-H. Meniai, Zinc removal from aqueous solutions by adsorption onto bentonite, Desalination Water Treat. 51 (2013) 5035–5048.
[82] S. Cheikh, A. Imessaoudene, J.-C. Bollinger, A. Hadadi, A. Manseri, A. Bouzaza, A. Assadi, A. Amrane, M. Zamouche, A. El Jery, Complete elimination of the ciprofloxacin antibiotic from water by the combination of adsorption–photocatalysis process using natural hydroxyapatite and TiO_2, Catalysts 13 (2023) 336.
[83] F. Sakr, A. Sennaoui, M. Elouardi, M. Tamimi, A. Assabbane, Étude de l'adsorption du Bleu de Méthylène sur un biomatériau à base de Cactus (Adsorption study of Methylene Blue on biomaterial using cactus), J. Mater. Environ. Sci. 6 (2015) 397–406.
[84] A.H. Jawad, K. Ismail, M.A.M. Ishak, L.D. Wilson, Conversion of Malaysian low-rank coal to mesoporous activated carbon: structure characterization and adsorption properties, Chin. J. Chem. Eng. 27 (2019) 1716–1727.
[85] Y. Han, X. Cao, X. Ouyang, S.P. Sohi, J. Chen, Adsorption kinetics of magnetic biochar derived from peanut hull on removal of Cr (VI) from aqueous solution: effects of production conditions and particle size, Chemosphere 145 (2016) 336–341.
[86] M. Zamouche, M. Chermat, Z. Kermiche, H. Tahraoui, M. Kebir, J.-C. Bollinger, A. Amrane, L. Mouni, Predictive model based on K-nearest neighbor coupled with the gray wolf optimizer algorithm (KNN_GWO) for estimating the amount of phenol adsorption on powdered activated carbon, Water 15 (2023) 493.
[87] H.N. Tran, S.-J. You, A. Hosseini-Bandegharaei, H.-P. Chao, Mistakes and inconsistencies regarding adsorption of contaminants from aqueous solutions: a critical review, Water Res. 120 (2017) 88–116.
[88] A. El Nemr, A.G. Shoaib, A. El Sikaily, A.E.-D.A. Mohamed, A.F. Hassan, Evaluation of cationic methylene blue dye removal by high surface area mesoporous activated carbon derived from ulva lactuca, Environmental Processes 8 (2021) 311–332.
[89] I. Aminu, S.M. Gumel, W.A. Ahmad, A.A. Idris, Adsorption isotherms and kinetic studies of Congo-red removal from waste water using activated carbon prepared from jujube seed, Am. J. Anal. Chem. 11 (2020) 47.
[90] Z. Ren, B. Jia, G. Zhang, X. Fu, Z. Wang, P. Wang, L. Lv, Study on adsorption of ammonia nitrogen by iron-loaded activated carbon from low temperature wastewater, Chemosphere 262 (2021) 127895.
[91] N. Hamri, A. Imessaoudene, N. Bouchelkia, R. Boudraa, S. Cheikh, J.-C. Bollinger, A.A. Assadi, A. Boukerroui, L. Mouni, Innovative surface modification of Kaolinite by direct grafting of an anionic surfactant to improve pollutant adsorption and effluent decontamination, J. Dispersion Sci. Technol. (2024) 1–20.
[92] A.H. Jawad, M. Bardhan, M.A. Islam, M.A. Islam, S.S.A. Syed-Hassan, S. Surip, Z. A. Alothman, M.R. Khan, Insights into the modeling, characterization and adsorption performance of mesoporous activated carbon from corn cob residue via microwave-assisted H_3PO_4 activation, Surf. Interfaces 21 (2020) 100688.
[93] E.C. Lima, A. Hosseini-Bandegharaei, J.C. Moreno-Piraján, I. Anastopoulos, A critical review of the estimation of the thermodynamic parameters on adsorption equilibria. Wrong use of equilibrium constant in the Van't Hoof equation for calculation of thermodynamic parameters of adsorption, J. Mol. Liq. 273 (2019) 425–434.
[94] X. Zhou, X. Zhou, The unit problem in the thermodynamic calculation of adsorption using the Langmuir equation, Chem. Eng. Commun. 201 (2014) 1459–1467.
[95] H.N. Tran, E.C. Lima, R.-S. Juang, J.-C. Bollinger, H.-P. Chao, Thermodynamic parameters of liquid–phase adsorption process calculated from different equilibrium constants related to adsorption isotherms: a comparison study, J. Environ. Chem. Eng. 9 (2021) 106674.
[96] J. Gao, Y. Liu, X. Li, M. Yang, J. Wang, Y. Chen, A promising and cost-effective biochar adsorbent derived from jujube pit for the removal of Pb (II) from aqueous solution, Sci. Rep. 10 (2020) 7473.
[97] M.A. Espinoza-Sanchez, K. Arevalo-Nino, I. Quintero-Zapata, I. Castro-Gonzalez, V. Almaguer-Cantu, Cr (VI) adsorption from aqueous solution by fungal bioremediation based using Rhizopus sp, J. Environ. Manag. 251 (2019) 109595.
[98] H.N. Tran, S.-J. You, H.-P. Chao, Thermodynamic parameters of cadmium adsorption onto orange peel calculated from various methods: a comparison study, J. Environ. Chem. Eng. 4 (2016) 2671–2682.
[99] N. Singh, G. Nagpal, S. Agrawal, Water purification by using adsorbents: a review, Environ. Technol. Innovat. 11 (2018) 187–240.
[100] R. Abdelazeem, H.A. Younes, Z.E. Eldin, A.A. Allam, H.A. Rudayni, S.I. Othman, A.A. Farghali, H.M. Mahmoud, R. Mahmoud, A selective, efficient, facile, and reusable natural clay/metal organic framework as a promising adsorbent for the removal of drug residue and heavy metal ions, Colloids and Interfaces 8 (2024) 50.
[101] H. Yazid, T. Bouzid, E.M. El Mouchtari, L. Bahsis, M. El Himri, S. Rafqah, M. El haddad, Insights into the adsorption of Cr (VI) on activated carbon prepared from walnut shells: combining response surface methodology with computational calculation, Cleanroom Technol. 6 (2024) 199–220.
[102] M.E. Peñafiel, J.M. Matesanz, E. Vanegas, D. Bermejo, R. Mosteo, M.P. Ormad, Comparative adsorption of ciprofloxacin on sugarcane bagasse from Ecuador and on commercial powdered activated carbon, Sci. Total Environ. 750 (2021) 141498.
[103] A. Stavrinou, C. Aggelopoulos, C. Tsakiroglou, Exploring the adsorption mechanisms of cationic and anionic dyes onto agricultural waste peels of banana, cucumber and potato: adsorption kinetics and equilibrium isotherms as a tool, J. Environ. Chem. Eng. 6 (2018) 6958–6970.
[104] L. Cui, C. Liu, G. Wu, Performance and mechanism of methylene blue biosorption on orange peel, Environ. Technol. 29 (2008) 1021–1030.
[105] V.-P. Dinh, H.M. Le, V.-D. Nguyen, V.-A. Dao, N.Q. Hung, L.A. Tuyen, S. Lee, J. Yi, T.D. Nguyen, L. Tan, Insight into the adsorption mechanisms of methylene blue and chromium (III) from aqueous solution onto pomelo fruit peel, RSC Adv. 9 (2019) 25847–25860.
[106] A. Hapiz, A.H. Jawad, L.D. Wilson, Z.A. Alothman, High surface area activated carbon from a pineapple (ananas comosus) crown via microwave-$ZnCl_2$ activation for crystal violet and methylene blue dye removal: adsorption optimization and mechanism, Int. J. Phytoremediation 26 (2024) 324–338.
[107] Y. Zhao, X. Liu, W. Li, S. Pei, Y. Ren, X. Li, C. Qu, C. Wu, J. Liu, Efficient and selective adsorption of cationic dye malachite green by Kiwi-peel-based biosorbents, Molecules 28 (2023) 5310.
[108] P. Makoś-Chełstowska, E. Słupek, J. Gębicki, Agri-food waste biosorbents for volatile organic compounds removal from air and industrial gases–A review, Sci. Total Environ. (2024) 173910.
[109] V. Chairgulprasert, H. Waehayee, Removal of methylene blue dye in water using longkong fruit peels, Applied Science and Engineering Progress 11 (2018) 287–295.
[110] A. Machrouhi, A. Elhalil, F.Z. Mahjoubi, H. Tounsadi, M.h. Sadiq, M. Abdennouri, Adsorption behavior of methylene blue onto powdered Ziziphus lotus fruit peels and Avocado kernels seeds, Journal of Applied Surfaces and Interfaces 1 (2017) 49–56.

[111] E.-K. Guechi, O. Hamdaoui, Biosorption of methylene blue from aqueous solution by potato (Solanum tuberosum) peel: equilibrium modelling, kinetic, and thermodynamic studies, Desalination Water Treat. 57 (2016) 10270–10285.
[112] F. Moubarak, R. Atmani, I. Maghri, M.h. Elkouali, M. Talbi, M.L. Bouamrani, M. Salouhi, A. Kenz, Elimination of methylene blue dye with natural adsorbent "banana peels powder", Glob. J. Sci. Front. Res. (GJSFR): B Chemistry 14 (2014) 39–44.
[113] A.H. Jawad, Y. Ngoh, K.A. Radzun, Utilization of watermelon (Citrullus lanatus) rinds as a natural low-cost biosorbent for adsorption of methylene blue: kinetic, equilibrium and thermodynamic studies, J. Taibah Univ. Sci. 12 (2018) 371–381.
[114] A.H. Jawad, A.M. Kadhum, Y. Ngoh, Applicability of dragon fruit (Hylocereus polyrhizus) peels as low-cost biosorbent for adsorption of methylene blue from aqueous solution: kinetics, equilibrium and thermodynamics studies, Desalination Water Treat. 109 (2018) 231–240.
[115] M. Boumediene, H. Benaïssa, B. George, S. Molina, A. Merlin, Characterization of two cellulosic waste materials (orange and almond peels) and their use for the removal of methylene blue from aqueous solutions, Maderas, Ciencia Tecnolog. 17 (2015) 69–84.